AN ANALYTICAL MODEL OF THE FREQUENCY DEPENDENT 3-D CURRENT SPREADING IN FORWARD BIASED SHALLOW RECTANGULAR P-N JUNCTIONS

A THESIS

submitted by

SHUBHAM JAIN

for the award of the degree

of

BACHELOR OF TECHNOLOGY
and
MASTER OF TECHNOLOGY

Department of Electrical Engineering
Indian Institute of Technology Madras, India

MAY 2016

THESIS CERTIFICATE

This is to certify that the report titled **"An Analytical Model of the Frequency Dependent 3-D Current Spreading in Forward Biased Shallow Rectangular P-N Junctions"**, submitted by **Shubham Jain,** to the Indian Institute of Technology Madras, for the award of the degrees of **Bachelor of Technology** in **Electrical Engineering** and **Master of Technology** in **Microelectronics and VLSI Design** is a bona fide record of the work done by him under our supervision. The contents of this thesis, in full or in parts, have not been submitted to any other Institute or University for the award of any degree or diploma.

Place: Chennai
Date: 12th May 2016

Research Guide

Prof. Shreepad Karmalkar
Professor
Dept. of Electrical Engineering
I.I.T. Madras, 600 036

ACKNOWLEDGEMENTS

I would like to express my sincere gratitude to my guide Prof. S. Karmalkar, for his prolific encouragement and guidance. I am grateful to him for his timely advice and constructive criticism which made the course of my project an excellent learning experience. The vast amount of time and energy spent by him in attending to my work made it possible for me to complete this work. I deeply desire to imbibe his qualities as a teacher, researcher and motivator.

My sincere thanks to Vijaya Kumar for his precious advice and support. Without his contributions this project would not have been realized. He was always available to help me whenever I found myself stuck, be it in devices, mathematics or simulation tool. I am also thankful to Anvar for all the insightful discussions we had on semiconductors. He helped me deepen my understanding of devices and my interest in the area. I can say that I learned a great deal from my lab mates Jaikumar sir, Sukalpa, Pradeep and Prasannanjaneyulu. I would also like to acknowledge Rekha who took out time from her busy schedule to answer my queries whenever I had a doubt.

I thank my parents for bringing me up with the best education and moral values and for enabling me to pursue my dreams. Thanks to my friends and siblings for their never-ending support at each and every point of my life.

ABSTRACT

KEYWORDS: p-n junction, semiconductor junction, current spreading, analytical model, ac equivalent circuit, current boundary conditions, forward bias, admittance, capacitance, conductance, two-dimensional flow, three-dimensional flow

Vijaya et al.[2] presented an analytical model of the frequency dependent spreading of the small-signal minority carrier flow in forward biased shallow p-n junctions, having stripe and circular geometries. The present work extends this approach to model a general rectangular junction encountered in practice. The junction could be eccentric and may have rounded corners or can have an ohmic or HI-LO back contact. The current spreading is expressed in terms of the junction length and width, lateral and vertical extent beyond the junction, diffusion length, lifetime, transit time, frequency and the surface recombination velocity at HI-LO contact. It is shown that the spreading in a circular junction approximates that in a square junction of the same area, and that in the direction of a side which is more than four times the diffusion length can be neglected. The model is validated using TCAD simulation.

TABLE OF CONTENTS

LIST OF TABLES

LIST OF FIGURES

NOTATION

V	Applied DC bias
$\tilde{v}$	Applied small-signal bias
Ψ	Potential Distribution
$\bar{I}$	Forward Current
$\tilde{\imath}$	Small-signal forward current
$\bar{J}_{pz}$	Normal DC hole current density
$\tilde{J}_{pz}$	Normal small-signal hole current density
J_p	Total hole current density
J_n	Total electron current density
p_e	Total excess hole density
$\bar{p}_e$	DC excess hole density
$\tilde{p}_e$	Small-signal excess hole density
G	Excess generation rate
R	Excess recombination rate
p_{n0}	Equilibrium hole density in the n-region
$\bar{F}_{2\text{-}D}, \bar{F}_{3\text{-}D}$	2D, 3D DC current spreading factor
$\tilde{F}_{2\text{-}D}, \tilde{F}_{3\text{-}D}$	2D, 3D small-signal current spreading factor
f	Frequency in Hz
ω	Frequency in rad/s
G_{diff}	Diffusion conductance
C_{diff}	Diffusion capacitance
C_{dep}	Depletion capacitance
g_{bn}, g_{bp}	n-region, p-region bulk conductance
C_{bn}, C_{bp}	n-region, p-region bulk capacitance
$R_{3\text{-}D}$	2D, 3D bulk spreading resistances
θ	Current spreading angle from the junction, degrees

V_{bi}	Built-in potential
q	Electronic charge
D_p	Hole diffusion co-efficient
μ_p	Hole mobility
L_p	Hole diffusion length
L_p^*	Complex hole diffusion length
τ_p	Hole lifetime
τ_d	Dielectric relaxation Lifetime
V_t	Thermal voltage
ρ	Space-charge
σ	Conductivity
μ	Permeability
ε_s	Dielectric permittivity of silicon
N_a	p-type doping
N_d	n-type doping
$2a$	Lateral extent of the junction
Δ	Lateral extent of the n-region beyond the junction on one-side
W	Vertical extent of the n-region

Chap 1. INTRODUCTION

Importance of P-N junctions cannot be overemphasized. They have undergone an extensive analysis in books as well as research papers. Most of the research in p-n junction has been undertaken by approximating the current flow to be one-dimensional due to the ease of solution. However a practical forward biased p-n junction consists of non-parallel current flow between the p and n contacts, smaller of which is located arbitrarily over the larger as shown in Fig. 1.1. This flow consists of both majority and minority carrier current. The minority carrier current occurs due to the concentration gradient (i.e. diffusion) whereas the majority carrier current occurs due to the potential gradient (i.e. drift).

The drift component has been analytically modelled extensively as spreading resistance; an extensive review of this work and a compact model is present in [1]. However analytical modelling of diffusion component is difficult because of the mixed boundary condition, i.e. Dirichlet and Neumann boundary conditions, present over the different regions containing the junction (top surface in Fig. 1.1). This limitation was recently overcome in [2], for p-n junction, by replacing the Dirichlet-Neumann mixed-boundary conditions on the top surface by a homogeneous Neumann boundary condition over the entire surface. This approach was used to successfully model stripe and circular geometries. It showed that, as frequency increases, the minority carrier current spreading reduces since this current occurs due to a combination of diffusion and recombination process.

Stripe or circular geometries do not represent a practical junction accurately. Hence, in the present work, we extend the approach of [2] to model 3-D minority carrier current spreading in a rectangular geometry. An analytical solution of the minority carrier continuity equation is used to develop a model for the DC and frequency dependent minority carrier current spreading in forward biased shallow rectangular p-n junctions with finite extent of semiconductor region beyond the junction. This model is then used to find current spreading in practical junctions which can be eccentric and can have rounded corners. Future scope is to find a compact expression for the infinite series solution presented in this report to improve computational speed.

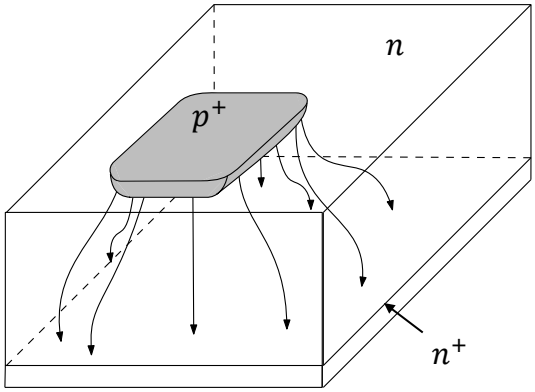

Fig. 1.1 Current spreading in practical forward biased p-n-n^+ junction

The thesis is organized as follows. Chapter 2 reviews the equations and approximations used for modelling the current in forward biased p-n junctions, briefly summarizes the prior work ([3] – [7]) on minority carrier spreading in practical forward biased junctions, and details the approach adopted by [2] which is the basis of the work presented in this thesis. Chapter Chap 3 presents our solutions for minority carrier and current distributions as well as the small-signal equivalent circuit for p^+-n junction with ohmic back contact. This chapter also validates our model against simulations and compares it with existing models. Chapter 4 gives a general model which can be used both for p^+-n and p^+nn^+ junction and verifies it against TCAD simulations. Chapter 5 gives conclusions and scope for future work.

Chap 2. REVIEW

In this chapter, we first review the basic semiconductor equations and their approximations for modelling forward current in diodes. Next, we briefly summarize the results and limitations of prior work that has addressed the issue of minority carrier spreading. Then we give a detailed review of a recent paper [2] on minority carrier spreading. Finally, we outline the objectives of our work in the light of the above review.

2.1 BASIC SEMICONDUCTOR EQUATIONS

In order to model the current-voltage characteristics of most semiconductor devices, following equations are used as the starting point:

the electron and hole continuity equations,

$$\frac{\partial n}{\partial t} - \frac{\Delta . J_n}{q} = G - R \qquad \frac{\partial p}{\partial t} + \frac{\Delta . J_p}{q} = G - R \tag{2.1}$$

the drift-diffusion current density equations,

$$J_n = q\mu_n nE + qD_n \Delta n \qquad J_p = q\mu_p pE - qD_p \Delta p \tag{2.2}$$

and the electrostatic equations,

$$\nabla^2 \psi = -\rho/\epsilon_s \tag{2.3}$$

where $\rho = q(p - n + N_D - N_A)$ and all symbols have their usual meaning.

2.2 APPROXIMATIONS AND EQUATIONS FOR MODELING FORWARD CURRENT OF DIODES

Listed below are the approximations used to achieve the ideal diode model.

Structure:

Junction is abrupt with uniform doping on both sides. Dopants are ionized completely.

Space-Charge Region

- Space charge region is fully depleted of mobile carriers.
- Recombination and generation in space charge region is neglected.
- Quasi-equilibrium conditions prevail, so that the Boltzmann approximation is valid throughout the space charge layer.

Quasi-Neutral Region

- Most of the applied voltage drops in the space charge region. Hence this region is field free and minority carrier current is only due to diffusion. This eliminates the poisson's equation and drift term from the current density equations.
- The applied bias is small enough to consider low injection level.
- No excess generation other than thermal means. This eliminates the excess generation term from the continuity equation.

High Frequency

- In small signal analysis, the AC voltage applied over DC bias is much smaller compared to V_t

Above approximations reduce the problem to a solution of just the hole distribution in the quasi-neutral n-region using the following equations

$$\frac{\partial p}{\partial t} + \frac{\Delta . J_p}{q} = -\frac{p_e}{\tau_p} \qquad J_p = -qD_p \Delta p_e \tag{2.4}$$

where $p_e = p_n - p_{n0}$, p_{n0} being the equilibrium concentration of holes in the n-region. Equation (2.4) can be combined into a single equation

$$\frac{\partial p_e}{\partial t} - D_P \nabla^2 p_e = -\frac{p_e}{\tau_p} \tag{2.5}$$

Under steady state DC conditions, (2.5) reduces to

$$\nabla^2 \bar{p_e} = \bar{p_e}/L_p^2 \qquad L_p = \sqrt{D_p \tau_p} \tag{2.6}$$

and for small signal the above equation can be modified as

$$\nabla^2 \bar{p_e} = \bar{p_e}/{L_p^*}^2 \qquad L_p^* = \frac{L_p}{\sqrt{1 + j\omega\tau_p}} \tag{2.7}$$

2.3 MODELS FOR DC/FREQUENCY DEPENDENT FORWARD CURRENT INCLUDING 2-D/3-D EFFECTS

2.3.1 Models of the last century [3]-[7]

Grimbergen[3] was the first one to consider spreading effects on minority carrier current in a p-n junction. He considered an epitaxial p^+nn^+ diode with circular junction and infinite lateral extent as shown in the Fig. 2.1(a). The 2-D problem is simplified by

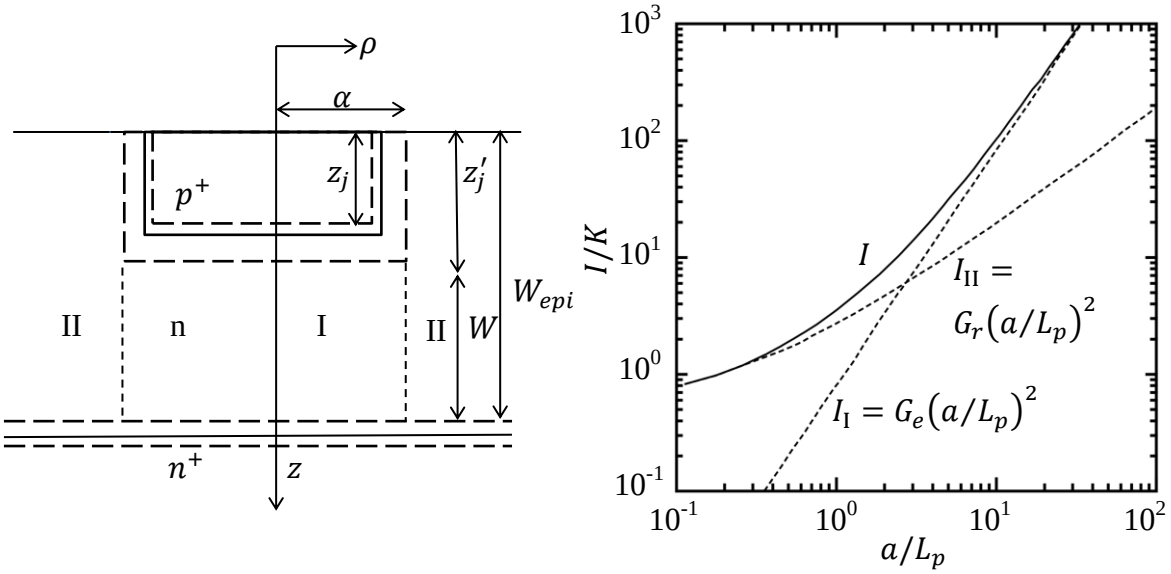

(a) (b)

Fig. 2.1 (a) Device cross-section modelled by Grimbergen [3]. (b) Normalized current and its components as a function of normalized junction radius.

assuming that excess hole density, p_e in region I is independent of radial co-ordinate r and gives rise to current component I_I and in region II is independent of z and gives current component I_{II}. The recombination velocity, S, of the HI-LO junction (i.e. nn^+ junction) and that of the oxide-silicon interface are taken zero.

Component I_1 and I_{II} are obtained by solving (2.6) assuming rectangular and cylindrical coordinates respectively

$$I_{\mathrm{I}} = q\, A\, \bar{p}_e(z_j') \frac{W}{\tau_p} \quad \text{where} \quad W = W_{epi} - z_j' < L_p \tag{2.8}$$

$$I_{\mathrm{II}} = q\, A\, \bar{p}_e(a) \frac{D_p}{L_p} \frac{2W_{epi}}{a} \frac{K_1(a/L_p)}{K_0(a/L_p)} \tag{2.9}$$

$A = \pi a^2$ is the junction area and $\bar{p}_e(a)$ is approximated by a mean value = $\bar{p}_e(z_j')$ for $W < L_p$. Finally, the total current I is expressed as

$$I = K\left((a/L_p)^2 G_e + (a/L_p)^2 G_r\right)$$

where (2.10)

$$K = q \frac{\bar{p}_e(z_j')}{\tau_p} W_{epi} L_p^2 \pi, G_e = \frac{W}{W_{epi}}, G_r = 2\left(\frac{a}{L_p}\right)^{-1} \frac{K_1(a/L_p)}{K_0(a/L_p)}$$

and G_e/G_r signifies the relative importance of the current component I_{II} as compared to

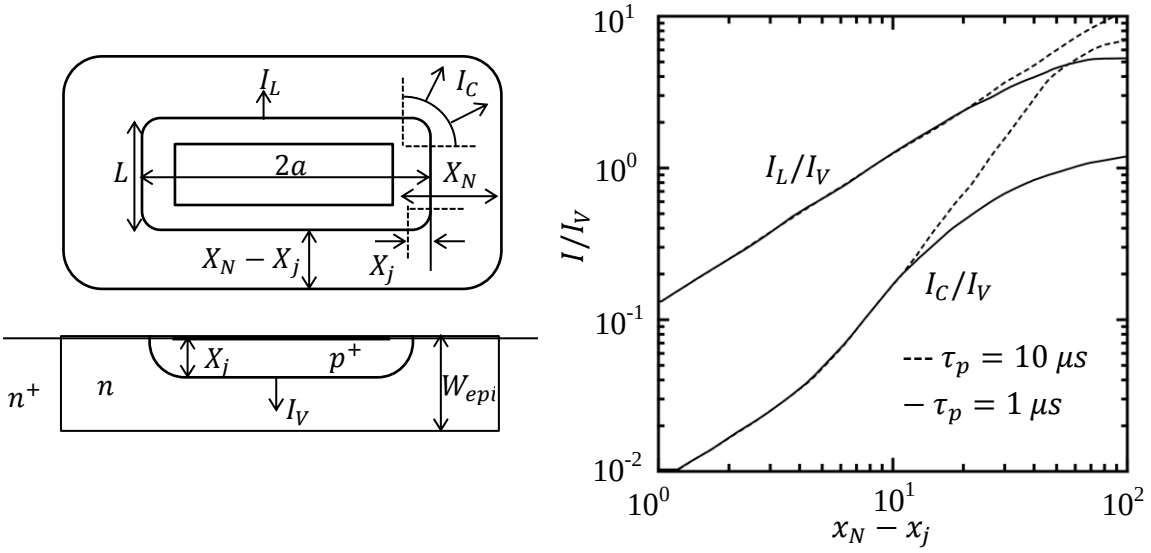

(a) (b)

Fig. 2.2 (a) Device cross-section modeled by Roulston et. al [5]. (b) Lateral and corner current normalized to vertical current as a function of the distance between the isolation walls and junction edge.

the current component I_{I}. Fig. 2.1(b) shows the current I and its components I_{I} and I_{II} as a function of junction radius in a normalized form.

Roulston et. al. extended this model by considering rectangular p^+-n-n^+ structures in [5] and further accounted for the effect of finite n^+ isolation walls in [4]. The top-view and the cross-section of the geometry considered is shown in Fig. 2.2(a). The hole surface recombination velocity is taken zero at the n-n^+ interface which is assumed to be equidistant from the p^+-n junction at all points along the periphery. The total current is divided into three independent components namely - I_V (vertical), I_L (lateral), I_C (corner). The vertical and lateral currents are obtained using a 1-D analysis and given by

$$I_V = q(2a \times L)\, p(0) \frac{(W_{epi} - x_j)}{\tau_p} \qquad \text{for } W_{epi} - x_j \ll L_p$$
$$I_L = q\left[2(2a + L)\, W_{epi}\right] p(0) \frac{(x_N - x_j)}{\tau_p} \qquad \text{for } x_N - x_j \ll L_p \tag{2.11}$$

where, $p(0)$ is the minority carrier concentration on the boundary of depletion region in n-region. Corner currents are evaluated by solving (2.6) in cylindrical coordinate system assuming a perfectly blocking (i.e. zero surface recombination velocity) n-n^+ interface. The solution was obtained by numerical integration by choosing an initial guess for the

hole current at $r = x_j$ and iterating on this value till the boundary condition at $r = x_N$ is satisfied. However, for a special case where the n^+ isolation wall is within one diffusion length of p^+n junction, I_C is solved analytically by letting $L_p \to \infty$ in the continuity equation (2.5) to get

$$I_C = q\left(x_N^2 - x_j^2\right) W_{epi} p(0)/\tau \tag{2.12}$$

Fig. 2.2(b) shows the importance of the lateral and corner currents relative to the vertical current as a function of the spacing between the junction and the n^+ isolation wall. It is seen that for a spacing > 10μm lateral current exceeds vertical current whereas corner current exceeds it for $\tau_p = 10\mu s$ and becomes a considerable fraction for $\tau_p = 1\mu s$.

Model by Heasell [6] took the same structure as Roulston and partitioned the junction into a plane, a quarter of cylinder (with axis as R_1R_2) and an octant of a sphere centered about R_2 shown in Fig. 2.3(a). Model replaced the iterative forward numerical integration scheme with analytical general solutions for carrier concentration and current for the plane or one-dimensional junction, as a reference device, as well as for the cylindrical and spherical junctions. The DC hole continuity equation (2.6) is solved in the n-region using the boundary conditions

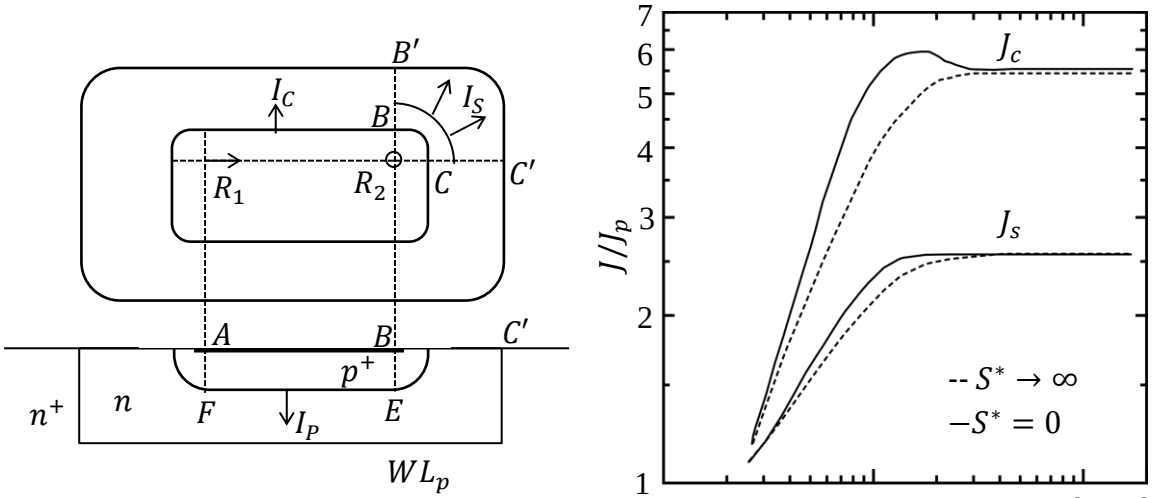

(a) (b)

Fig. 2.3 (a) Device cross-section modelled by Heasell [6] (b) Current density in a Spherical/Cylindrical junction as compared to a planar junction.

$$p_e = p_e(\mathrm{W}_0) \text{ at } \mathrm{z} = \mathrm{W}_0 \quad \text{and} \quad \nabla p_e = -S^* p_e(\mathrm{W}) \text{ at } \mathrm{z} = \mathrm{W} \tag{2.13}$$

where W_0 is the edge of depletion region in n-region and S^* is recombination velocity S at the outer boundary W normalized as SL_p/D_p . All lengths are normalised with respect to hole diffusion length L_p. The general solutions for the current densities J_p, J_c and J_s arising from the plane, cylindrical and spherical junctions respectively, normalized to the 1-D current density J_o of a long diode, are given by

$$\frac{J_p(\mathrm{z})}{J_o} = \frac{(1+S^*)\exp(\mathrm{W}-\mathrm{z}) - (1-S^*)\exp\{-(\mathrm{W}-\mathrm{z})\}}{(1+S^*)\exp(\mathrm{W}-\mathrm{W}_0) - (1-S^*)\exp\{-(\mathrm{W}-\mathrm{W}_0)\}} \tag{2.14}$$

$$\frac{J_c(\mathrm{z})}{J_o} = \frac{K_1(\mathrm{z})[(I_1(\mathrm{W}) + S^* I_0(\mathrm{W})] - I_1(\mathrm{z})[(K_1(\mathrm{W}) - S^* K_0(\mathrm{W})]}{K_0(\mathrm{W}_0)[(I_1(\mathrm{W}) + S^* I_0(\mathrm{W})] + I_0(\mathrm{W}_0)[(K_1(\mathrm{W}) - S^* K_0(\mathrm{W})]} \tag{2.15}$$

where K_0, I_0, K_1, I_1 are modified Bessel functions of the second kind, and

$$\frac{J_s(\mathrm{z})}{J_o} = \frac{\mathrm{W}_0\{(\mathrm{z}+1)[\mathrm{W}(1+S^*)-1]\exp(\mathrm{W}-\mathrm{z}) - (\mathrm{z}-1)[\mathrm{W}(1-S^*)+1]\exp-(\mathrm{W}-\mathrm{z})\}}{\mathrm{z}^2\{[\mathrm{W}(1+S^*)-1]\exp(\mathrm{W}-\mathrm{W}_0) + [\mathrm{W}(1-S^*)+1]\exp-(\mathrm{W}-\mathrm{W}_0)\}} \tag{2.16}$$

Fig. 2.3(b) shows the relative values of current density in cylindrical and spherical junction to a planar junction for a junction depth of W_0 = 0.2μm. It also shows the difference in current values for two extreme recombination velocities.

Every model discussed so far obtained a solution by splitting the device into independent components and thus they have failed to give a correct estimate of the current spreading. Chen et. al. [7] in their work obtained an analytical solution for the two dimensional boundary value problem by reducing it to a pair of dual integral equations by applying Hankel transformation to the boundary condition. The diode structure considered is circular junction with infinite lateral extent and a shallow p-region of radius

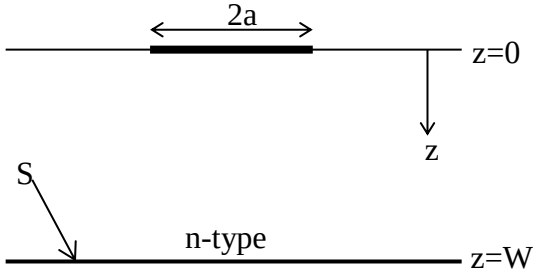

Fig. 2.4 Device cross-section modelled by Chen et.al [7].

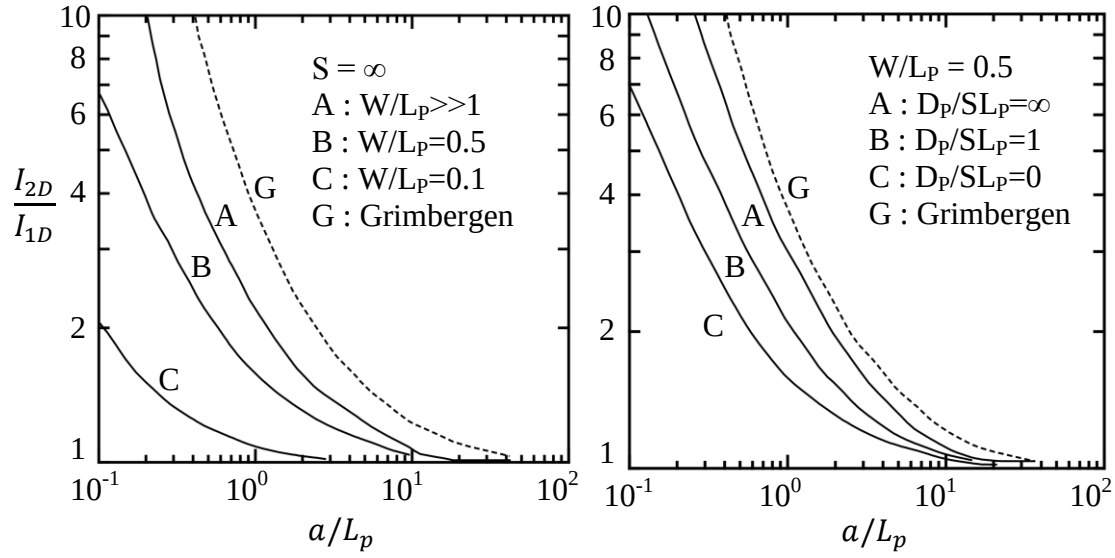

Fig. 2.5 Current spreading as a function of normalized junction radius for different W/L_p and S

a, as shown in Fig. 2.4. Equation (2.6) is solved using a cylindrical co-ordinate system, assuming no variation of the excess carrier concentration p_e along the azimuthal direction, and using the following boundary conditions,

$$\begin{aligned} \bar{p}_e(\mathrm{r},0) &= \bar{p}_e(x_j) \qquad 0 \le \mathrm{r} \le 1 \\ \frac{\partial \bar{p}_e(\mathrm{r},0)}{\partial \mathrm{z}} &= 0 \qquad 1 \le \mathrm{r} \le \infty \\ D_P \frac{\partial \bar{p}_e(\mathrm{r},W)}{\partial \mathrm{z}} &= -S\,\bar{p}_e(\mathrm{r},W) \end{aligned} \tag{2.17}$$

Here, r is the radial co-ordinate ρ normalized with respect to the junction radius a, i.e. $\rho = \mathrm{r}a$, $\bar{p}_e(x_j)$ is the excess carrier concentration at the depletion edge and S is the recombination velocity at the bottom surface of the n-region. Final solution for the 2-D hole diffusion current $I_{2\text{-}D}$ is given as

$$I_{2\text{-}D} = \sqrt{8\pi}\, q D_p a\, a_0$$

where

$$a_0 + \sum_{m=0}^{\infty} L_{m0} a_m = \sqrt{\frac{2}{\pi}}\,\bar{p}_e(x_j) \qquad a_n + \sum_{m=0}^{\infty} L_{mn} a_m = 0 \quad \text{for} \quad n > 0 \tag{2.18}$$

L_{mn} is a function of a/L_p , D_p and S and is calculated numerically. Fig. 2.5(a) shows the current spreading factor $I_{2\text{-}D}/I_{1\text{-}D}$ as a function of the junction radius a, assuming a perfectly absorbing back surface i.e. $S = \infty$. Fig. 2.5(b) compares the spreading factor for

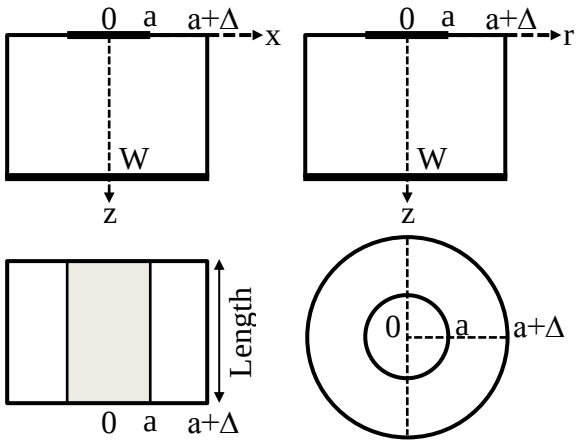

Fig. 2.6 Top-view and side-view of stripe and circular geometry

different values of S and we can see that current spreading increases with decreasing S. Here, $I_{1\text{-}D}$ is obtained from the known formula for a 1-D p-n junction. The two-dimensional current spreading is found to be significantly high for $a/L_p < 10$ and large W/L_p. Even though this model solved the whole device as a single unit it considered infinite lateral extent which is an impractical case.

2.3.2 Recent Model by Vijaya et. al. [2]

This model forms the basis for our model. It discusses DC and small signal current spreading in 2-D/3-D finite-sized(both vertically and laterally) shallow stripe and circular p-n junctions. Current flow in shallow p-region is assumed 1-D and calculated using available formulas. The structure is idealized by assuming a disk shaped p-region as shown in Fig. 2.6. Bottom contact is assumed ohmic i.e. surface recombination velocity is infinite.

Solution methodology used by this model is to replace the mixed (Neumann+Dirichlet) boundary condition on top surface by a homogeneous(Neumann) boundary condition. Current in stripe and circular shaped junctions is calculated by solving (2.6), in rectangular and cylindrical polar coordinates respectively, with following boundary conditions on top surface

$$\left.\frac{\partial p_e}{\partial z}\right|_{z=0} = \begin{cases} \dfrac{J_{pz}}{qD_p} & \text{if } x, \rho \le a \\ 0 & \text{elsewhere} \end{cases} \tag{2.19}$$

It assumes that the current density at the top contact is uniform. Solving for current with given assumption we get

$$\bar{J}_{pz} = \frac{Fqp_{n_0}D_p}{L_p}(\exp(V/V_t) - 1)\coth(W/L_p)$$ where F can be

$$F_{2\text{-}D}{}^{-1} = \left(\frac{a}{a+\Delta}\right) + 2\sum_{n=1}^{\infty} \frac{\sin\left(\frac{n\pi a}{a+\Delta}\right)\cos\left(\frac{n\pi c}{a+\Delta}\right)}{n\pi\sqrt{1+\left(\frac{n\pi L_p}{a+\Delta}\right)^2}} \tanh\left(\sqrt{1+\left(\frac{n\pi L_p}{a+\Delta}\right)^2}\frac{W}{L_p}\right)\coth\left(\frac{W}{L_p}\right) \tag{2.20}$$

$$F_{3\text{-}D}{}^{-1} = \left(\frac{a}{a+\Delta}\right)^2 + \frac{2a}{(a+\Delta)^2}\sum_{n=1}^{\infty}\frac{1}{\sqrt{1+\left(k_nL_p\right)^2}}\left(\frac{1}{k_n}\right)\left(\frac{J_1(k_na)*J_0(k_nc)}{J_0{}^2(k_n\,(a+\Delta))}\right)\tanh\left(\sqrt{1+\left(k_nL_p\right)^2}\,\frac{W}{L_p}\right)\coth\left(\frac{W}{L_p}\right)$$

where $c = 0.8a$ is the point on the junction where junction law is applied.

The model also gives the small signal spreading factor, F^* which is $F_{2\text{-}D}$ or $F_{3\text{-}D}$ with L_p replaced by L_p^* and predicts that the spreading gets restricted as the frequency is increased. Further it models small signal behaviour of stripe and circular junctions. The equivalent circuit is given in Fig. 2.7 and remains same for the case of 1-D, 2-D and 3-D geometry. Here, G_{dif} and G_s are the diffusion and series conductance, and C_{dif}, C_{dep}, and C_s are the diffusion, depletion, and series capacitances, all per unit area of the 1-D junction; the ratio C_s/G_s = dielectric relaxation time,τ_d. Here $G_{dif} = G_{ndif} + G_{pdif}$ and $C_{dif} = C_{ndif} + C_{pdif}$ where G_{ndif} and C_{ndif} are in shallow p-region and are given by 1-D formulas. G_{pdif} and C_{pdif} are found using the fact that y_{pdif} is ratio of small signal current $\tilde{j}_{pz}$ to small signal voltage $\tilde{v}$. $\tilde{j}_{pz}$ is written as $\tilde{v}/V_t$ times $\bar{J}_{pz}$ given by (2.20) with F/L_p replaced by F^*/L_p^*. Expression for G_s includes majority carrier spreading by assuming DC conditions up to the frequency for which skin depth $(1/\pi f\mu\sigma)^{1/2}$ in n-region remains much larger than its lateral dimension $(a+\Delta)$. Spreading resistance formula for stripe and circular geometries are taken from

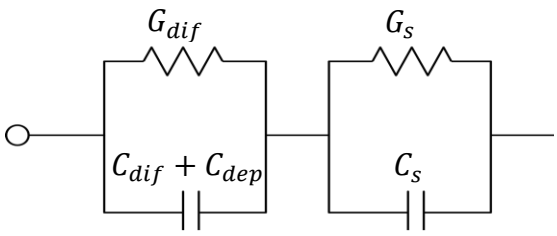

Fig. 2.7 Small signal equivalent of a p-n junction diode

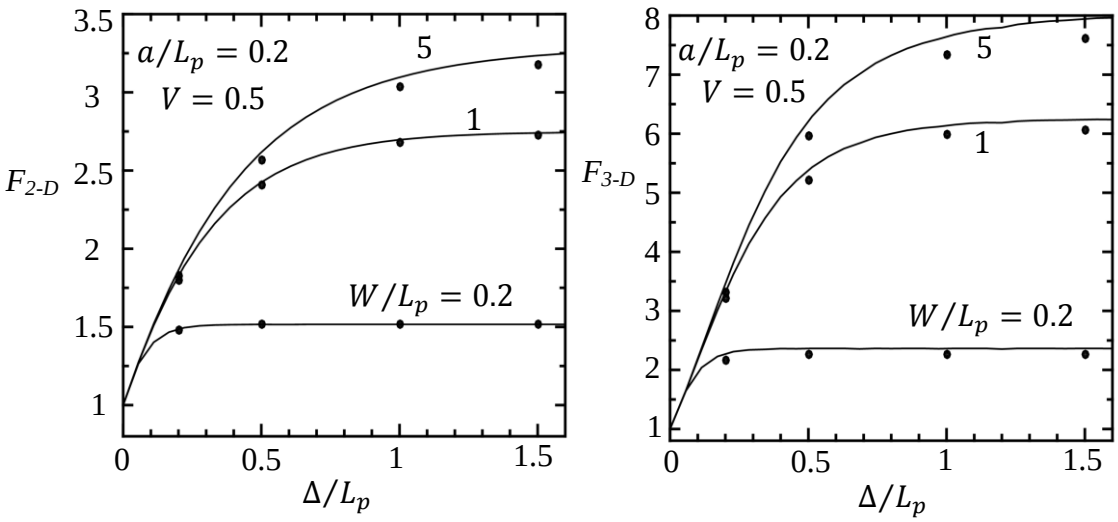

Fig. 2.8 DC current spreading factor in (a) Stripe-shaped (b) Circular junction

[1](Table II) and $C_s = G_s\tau_d$. It is seen that at high frequencies majority carrier spreading plays a dominant role. For C_{dep} formula given in [8](29) has been used to include the effect of inversion layers formed in highly assymmetrical junctions.

Model predicts DC results within 7 % error as shown in Fig. 2.8 and small signal results within 16% error. Model also gives a method to predict current in a practical junction by taking 2-D effects along the edges and 3-D effects at the corners.

Major limitation of the model is that the geometries considered are not practical. The equivalent model provided for a practical junction distributes the current into two independent parts which can give rise to major limitations. The paper doesn't give any comparison of the equivalent method with numerical simulations or experimental results. Another shortcoming is that the results are given only for the case of perfectly absorbing bottom contact, whereas models discussed previously gave general solutions as function of surface recombination velocity at bottom surface of n-region.

2.4 OBJECTIVES OF THE PRESENT WORK

We aim to propose an analytical model for DC and frequency dependent minority carrier current spreading in a rectangular p-n junction. To be able to predict current values in a rectangular eccentric junction with rounded corners using rectangular junction. And to give a general model which uses the surface recombination velocity at bottom of n-region as a parameter to give spreading values.

Chap 3. MODEL FOR A JUNCTION WITH OHMIC BACK CONTACT

Vijaya et. al.[2] considered stripe and circular shapes for their amenability to a simple analytical solution. We consider a rectangular shaped junction for the practicality of the solution. We work with a junction where the p-region is shallow and n-region is long and focus on the 3-D current spreading in the n-region. The shallowness of the p-region allows three simplifications. First, the current flow from the vertical side walls of this region can be neglected. Second, the horizontal junction depletion edge in the n-region can be assumed to be in the same plane as the top of the n-region outside the junction area (see Fig. 3.1(a)). Third, the current flow in the p-region becomes 1-D for which models are available already.

We consider concentric and eccentric junctions with both sharp and rounded corners. In the case of the concentric structure, the geometric parameters of the model are: lateral extents of the p-region $2a_x$, $2a_y$ and those of the n-region beyond the junction edge Δ_x, Δ_y, vertical extent W of the n-region beyond the junction depth; the process parameters of the

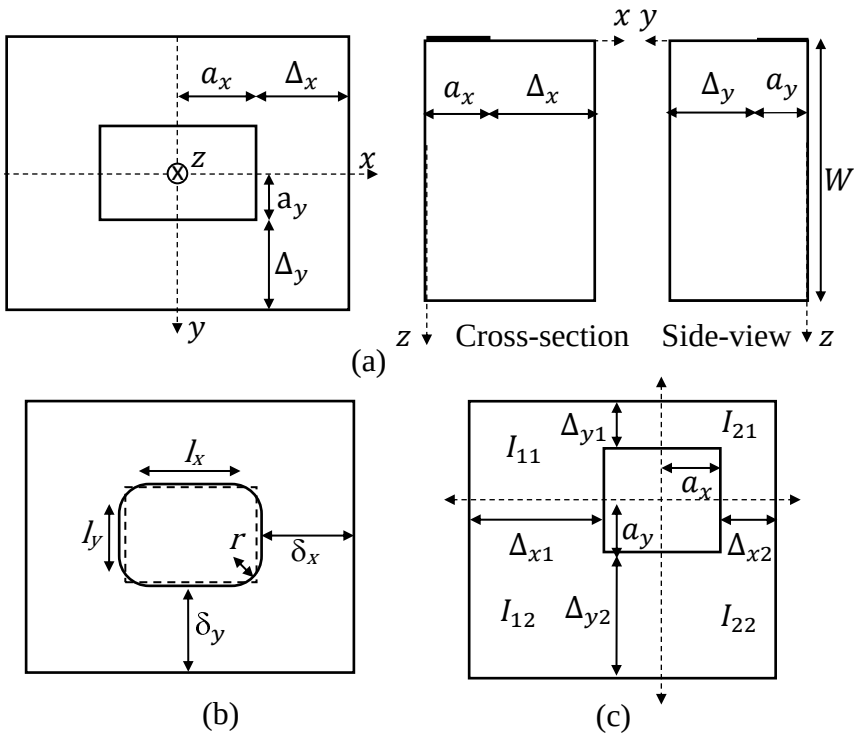

Fig. 3.1 (a) Top view of an idealized concentric rectangular p-n junction geometry considered in modeling, together with the cross- section and side view of a quarter of the structure. (b) Top view of an eccentric junction. (c) Top view of a concentric junction with rounded corners.

model are: uniform doping levels N_a on p-side and N_d on n-side, diffusion coefficient, lifetime of minority carriers - D_n, τ_n on p-side and D_p, τ_p on n-side; the constants employed in the model are electronic charge q, thermal voltage V_t and substrate dielectric constant, ε_s**.** The bottom contact is assumed to be ohmic, and the remaining boundary of the n-region to be well passivated so that the surface recombination velocity is zero.

Symmetry of the concentric structure about the vertical planes $x = 0$ and $y = 0$ allows us to work with just any one of the four quarters of the structure. We model the junction with rounded corners in terms of a junction having the same area but sharp corners, and an eccentric junction as a parallel combination of quarters of four different concentric structures.

3.1 EQUATIONS, BOUNDARY CONDITIONS AND APPROXIMATIONS

Consider a junction forward biased by DC voltage V on which a small-signal voltage of $\tilde{v} = \hat{v}e^{j\omega t}$ is superposed. Write the excess hole concentration for this situation as $p_e = \bar{p}_e + \tilde{p}_e$ where $\bar{p}_e$ is the DC part and $\tilde{p}_e = \hat{p}_e e^{j\omega t}$ is the small-signal part. In keeping with the ideal diode model, we assume low level injection and minority carrier flow due to diffusion. The latter assumption is valid even for frequencies where the majority carrier current distribution is influenced by skin effects. This is because the secondary drift current created by induced time-varying electric field accompanying the time-varying magnetic field is large in the case of majority carriers but rather small in the case of minority carriers. Under these conditions, the hole continuity equation can be separated into DC and small-signal parts as follows [(e.g. see [9])

$$\nabla^2\bar{p}_e = \frac{\bar{p}_e}{L_p^2} \qquad \nabla^2\tilde{p}_e = \frac{\tilde{p}_e}{L_p^{*2}} \qquad L_p^* = \frac{L_p}{\sqrt{1 + j\omega\tau_p}} \qquad (1)$$

where $\nabla^2 = \partial^2/\partial x^2 + \partial^2/\partial y^2 + \partial^2/\partial z^2$ and L_p^* is called the complex diffusion length. Clearly, the solution for small-signal $\tilde{p}_e$ is obtained from that of DC $\bar{p}_e$ by simply replacing L_p by L_p^*. Hence, we shall present the solution for the DC case and extend it to derive the small-signal conductance and capacitance.

Consider a quarter of the concentric structure described by the equations $x \geq 0$, $y \geq 0$ and $z \geq 0$.We have the boundary conditions $\bar{p}_e = 0$ over the ohmic bottom contact, and $\partial\bar{p}_e/\partial x = 0$ on the two vertical planes at $x = 0$, $x = a_x + \Delta_x$ and $\partial\bar{p}_e/\partial x = 0$ on the

two vertical planes at $y = 0$ and $y = a_y + \Delta_y$. On the top plane $z = 0$, we have a mixed-boundary condition as follows. Over the n-surface beyond the junction area, i.e. for $a_x \le x \le a_x + \Delta_x$ and $a_y \le y \le a_y + \Delta_y$, the surface recombination velocity is zero**,** so that the normal component of the current density is zero. This translates to the Neumann condition $\partial \bar{p}_e / \partial z = 0$ since the current is due to diffusion. On the other hand, over the junction area $0 \le x \le a_x$ and $0 \le y \le a_y$, we have the Dirichlet condition $\bar{p}_e = p_{n0}\left(e^{V/V_t} - 1\right)$ as per the law of the junction. Since this mixed-boundary condition creates difficulties in analytical solution, we replace the Dirichlet condition over the junction area by a condition on $\partial \bar{p}_e / \partial z$ so as to have a homogeneous Neumann condition over the entire $z = 0$ plane. This is achieved by assuming that the normal hole current density $\bar{J}_{pz}$ over the junction area is uniform, which amounts to a uniform $\partial \bar{p}_e / \partial z = -\bar{J}_{pz} / qD_p$ since the hole current is due to diffusion. This approximation is illustrated in Fig. 3.2.

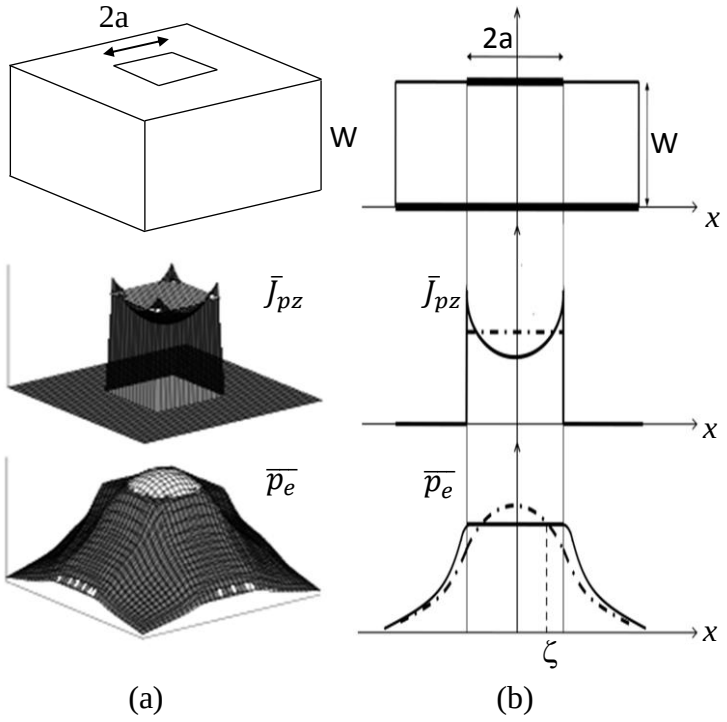

Fig. 3.2(a) Spatial distribution of the normal hole current density $\bar{J}_{pz}$ and hole density $\overline{p_e}$ over the junction area of an idealized square p-n junction.(b) Cross-section of (a) showing results of mixed boundary conditions (solid lines) and homogeneous Neumann boundary condition (dash-dotted lines).

This condition is valid up to the frequency for which the skin depths in the semi-conductor region above the junction and in the top metal contact remain much larger than the lateral dimensions a_x and a_y of these regions (see [2] for more details).

3.2 SOLUTION FOR THE DC FORWARD CURRENT

3.2.1 Concentric junction with sharp corners

We may rewrite (3.5) assuming a rectangular co-ordinate system as,

$$\frac{\partial^2 \bar{p}_e}{\partial x^2} + \frac{\partial^2 \bar{p}_e}{\partial y^2} + \frac{\partial^2 \bar{p}_e}{\partial \mathrm{z}^2} = \frac{\bar{p}_e}{L_p^2} \tag{3.1}$$

We solve the above equation by method of separation of variables (Fourier method), the solution to (3.1) can be expressed as,

$$\bar{p}_e(x, \mathrm{y}, \mathrm{z}) = \bar{p}_e(x) \times \bar{p}_e(\mathrm{y}) \times \bar{p}_e(\mathrm{z}) \tag{3.2}$$

For sake of simplicity we replace the terms in R.H.S as

$$p_e(x) \to X \qquad p_e(y) \to Y \qquad p_e(z) \to Z \implies \bar{p}_e(x, \mathrm{y}, \mathrm{z}) = X.Y.Z \tag{3.3}$$

Thus (3.1) can be rewritten in the form

$$\frac{X''}{X} + \frac{Y''}{Y} + \frac{Z''}{Z} = \frac{1}{L_p^2} \tag{3.4}$$

To obtain a solution to the above equation we replace L.H.S with sum of three constants whose sum is equal to $1/L_p^2$,

$$\frac{X''}{X} = -\lambda_1^2 \tag{3.5}$$

$$\frac{Y''}{Y} = -\lambda_2^2 \tag{3.6}$$

$$\frac{Z''}{Z} = \lambda_1^2 + \lambda_2^2 + \frac{1}{L_p^2} \tag{3.7}$$

where λ_1^2, λ_2^2 are positive constants.

General solution of (3.5) can be written as

$$X = A\sin(\lambda_1 x) + B\cos(\lambda_1 x) \tag{3.8}$$

However the sine term in above equation will not satisfy the boundary conditions in *x*, so we are left with

$$X = B\cos(\lambda_1 x) \quad \text{where} \quad \lambda_1 = \frac{n_1\pi}{a_x + \Delta_x} \text{ and } n_1 = 0,1,2,3\ldots..\infty \tag{3.9}$$

Similarly in *y* direction we can write the solution as

$$Y = C\cos(\lambda_2 y) \quad \text{where} \quad \lambda_2 = \frac{n_2\pi}{a_y + \Delta_y} \text{ and } n_2 = 0,1,2,3\ldots..\infty \tag{3.10}$$

The general solution of (3.7) will have hyperbolic sine and cosine terms. But the cosine term will not satisfy the boundary condition on the bottom contact/boundary, so we omit it to get

$$Z = E\sinh\left(\sqrt{\lambda_1^2 + \lambda_2^2 + \frac{1}{L_p^2}}\,(W - z)\right) \tag{3.11}$$

Thus the general solution for p_e can be written as the linear sum of all the combinations of *X.Y.Z* and is given as

$$p_e(x,y,z) = \sum_{n_1=0}^{\infty}\sum_{n_2=0}^{\infty} A_{n_1n_2}\cos(\lambda_1 x)\cos(\lambda_2 y)\frac{\sinh\left(\sqrt{\lambda_1^2 + \lambda_2^2 + \frac{1}{L_p^2}}\,(W - z)\right)}{\cosh\left(\sqrt{\lambda_1^2 + \lambda_2^2 + \frac{1}{L_p^2}}\,(W)\right)} \tag{3.12}$$

where $A_{n_1n_2}$ is the constant of summation. Here, the "cosh" term has been introduced for mathematical convenience as will be seen shortly. This general solution satisfies boundary conditions of section 3.3, on all boundaries except the top surface. We need to obtain $A_{n_1n_2}$ such that,

$$\frac{\partial p_e(x,y,z)}{\partial z}|_{z=0} = -\sum_{n_1=0}^{\infty}\sum_{n_2=0}^{\infty} A_{n_1n_2}\cos(\lambda_1 x)\cos(\lambda_2 y)\left(\sqrt{\lambda_1^2 + \lambda_2^2 + \frac{1}{L_p^2}}\right) \tag{3.13}$$

For sake of simplicity we replace R.H.S of above equation with a general function $f(x,y)$. We use this equation to extract the coefficients $A_{n_1n_2}$, which as a result of

introducing the "cosh" term doesn't contain any hyperbolic functions. We multiply (3.13) with $\cos\left(\frac{m_1\pi x}{a+\Delta}\right)$ on both sides and integrate over the range, $0 \le x \le a + \Delta$.

$$\int_0^{a_x+\Delta_x} f(x,y)\cos\left(\frac{m_1\pi x}{a_x+\Delta_x}\right)dx$$
$$= -\sum_{n_1=0}^{\infty}\sum_{n_2=0}^{\infty} A_{n_1n_2}\cos\frac{n_1\pi y}{a_y+\Delta_y}\left(\sqrt{\lambda_1^2+\lambda_2^2+\frac{1}{L_p^2}}\right)\int_0^{a_x+\Delta_x}\cos\frac{n_1\pi x}{a_x+\Delta_x}\cos\frac{m_1\pi x}{a_x+\Delta_x}dx \quad (3.14)$$

The integral on the RHS of this equation reduces to 0 for all $m_1 \neq n_1$ and for all $m_1 = n_1 \neq 0$ it reduces to $\frac{a_x+\Delta_x}{2}$ and we get

$$\int_0^{a_x+\Delta_x} f(x,y)\cos\frac{n_1\pi x}{a_x+\Delta_x}dx$$
$$= -\sum_{n_2=0}^{\infty} A_{n_1n_2}\cos\frac{n_1\pi y}{a_y+\Delta_y}\left(\sqrt{\lambda_1^2+\lambda_2^2+\frac{1}{L_p^2}}\right)\frac{a_x+\Delta_x}{2} \quad (3.15)$$

Repeating the same procedure for y we get

$$\int_0^{a_y+\Delta_y}\int_0^{a_x+\Delta_x} f(x,y)\cos(\lambda_1 x)\cos(\lambda_2 y)dxdy$$
$$= -A_{n_1n_2}\left(\sqrt{\lambda_1^2+\lambda_2^2+\frac{1}{L_p^2}}\right)\frac{a_x+\Delta_x}{2}\frac{a_y+\Delta_y}{2} \quad (3.16)$$

Setting

$$f(x,y) = \begin{cases}\frac{J_{pz}}{qD_p} & \text{if } x \le a_x \text{and } y \le a_y \\ 0 & \text{elsewhere}\end{cases} \quad (3.17)$$

and solving for $A_{n_1n_2}$ we get

$$A_{n_1n_2} = \frac{\frac{4J_{pz}}{qD_p/L_p}\sin(\lambda_1 a_x)\sin(\lambda_2 a_y)}{n_1n_2\pi^2\left(\sqrt{(\lambda_1 L_p)^2+(\lambda_2 L_p)^2+1}\right)} \text{ for } n_1, n_2 \neq 0 \quad (3.18)$$

To solve for $n_1 = 0, n_2 \neq 0$ we put $n_1 = m_1 = 0$ in (3.14) and keep rest of the solution same we get

$$A_{n_2} = \frac{a_x}{(a_x+\Delta_x)}\frac{\frac{2J_{pz}}{qD_p/L_p}\sin(\lambda_2 y)}{n_2\pi\left(\sqrt{(\lambda_2 L_p)^2+1}\right)} \quad (3.19)$$

Similarly for $n_2 = 0, n_1 \neq 0$ we get

$$A_{n_1} = \frac{a_y}{(a_y + \Delta_y)} \frac{\frac{2J_{pz}}{qD_p/L_p}\sin(\lambda_1 x)}{n_1\pi\left(\sqrt{(\lambda_1 L_p)^2 + 1}\right)} \tag{3.20}$$

Finally by solving for $n_1 = n_2 = 0$ we get

$$A = \frac{J_{pz}}{qD_p/L_p} \frac{a_x}{(a_x + \Delta_x)} \frac{a_y}{(a_y + \Delta_y)} \tag{3.21}$$

Substituting A, A_{n_1}, A_{n_2} and $A_{n_1 n_2}$ in the general solution (3.12), we obtain the hole distribution in the n-region as,

$$\begin{aligned} p_e(x, y, \mathrm{z}) = A\frac{\sinh\big((W-z)/L_p\big)}{cosh\big(W/L_p\big)} + \sum_{n_1=1}^{\infty} A_{n_1}\cos(\lambda_1 x)\frac{\sinh\left(\sqrt{\lambda_1^2 + \frac{1}{L_p^2}}(W-z)\right)}{\cosh\left(\sqrt{\lambda_1^2 + \frac{1}{L_p^2}}(W)\right)} \\ + \sum_{n_2=1}^{\infty} A_{n_2}\cos(\lambda_2 y)\frac{\sinh\left(\sqrt{\lambda_2^2 + \frac{1}{L_p^2}}(W-z)\right)}{\cosh\left(\sqrt{\lambda_2^2 + \frac{1}{L_p^2}}(W)\right)} \\ + \sum_{n_1=1}^{\infty}\sum_{n_2=1}^{\infty} A_{n_1 n_2}\cos(\lambda_1 x)\cos(\lambda_2 y)\frac{\sinh\left(\sqrt{\lambda_1^2 + \lambda_2^2 + \frac{1}{L_p^2}}(W-z)\right)}{\cosh\left(\sqrt{\lambda_1^2 + \lambda_2^2 + \frac{1}{L_p^2}}(W)\right)} \end{aligned} \tag{3.22}$$

Where

$$A = \frac{J_{p_z}}{qD_p/L_p} \frac{a_x}{(a_x + \Delta_x)} \frac{a_y}{(a_y + \Delta_y)}$$

$$A_{n_1} = \frac{a_y}{(a_y + \Delta_y)} \frac{\frac{2J_{p_z}}{qD_p/L_p}\sin(\lambda_1 a_x)}{n_1\pi\left(\sqrt{(\lambda_1 L_p)^2 + 1}\right)}$$

$$A_{n_2} = \frac{a_x}{(a_x + \Delta_x)} \frac{\frac{2J_{p_z}}{qD_p/L_p}\sin(\lambda_2 a_y)}{n_2\pi\left(\sqrt{(\lambda_2 L_p)^2 + 1}\right)}$$

$$A_{n_1 n_2} = \frac{\frac{4J_{pz}}{qD_p/L_p}\sin(\lambda_1 a_x)\sin(\lambda_2 a_y)}{n_1 n_2 \pi^2 \left(\sqrt{(\lambda_1 L_p)^2 + (\lambda_2 L_p)^2 + 1}\right)}$$

To solve for $\bar{J}_{pz}$ using the above equation, we need to relate $\bar{p}_e$ to the applied voltage V using the junction law. However, $\bar{p}_e$ varies over the junction area because of the uniform $\partial\bar{p}_e/\partial z$ condition imposed over this region to obtain solution for $\bar{p}_e$(see Fig. 3.2). Therefore, a question arises regarding the location over the junction where the junction law should be applied. Following [2], we use a location $(x, y) = (\zeta a_x, \zeta a_y)$ which matches the analytically determined value of the current $4a_x a_y \bar{J}_{pz}$ to the accurate value determined numerically based on the mixed boundary condition on the top surface. Thus, we solve for $\bar{J}_{pz}$ by setting $\bar{p}_e(\zeta a_x, \zeta a_y, 0) = p_{n0}\left(e^{\frac{V}{V_t}} - 1\right)$ in (3.22). Our mixed boundary condition simulations for a wide range of device dimensions establish that $\zeta = 0.8$ which is same as the value used for a stripe shaped junction in [2]. We express $\bar{J}_{pz}$ as the product of a current spreading factor $F_{3\text{-}D}$ and the current density under 1-D conditions, i.e,

$$\bar{J}_{pz} = F_{3\text{-}D}\left[\frac{qD_p}{L_p}\, p_{n0}\left(e^{\frac{V}{V_t}} - 1\right)\right]\coth\left(\frac{W}{L_p}\right) \tag{3.23}$$

From (3.22), (3.23) and $\bar{p}_e(\zeta a_x, \zeta a_y, 0) = p_{n0}\left(e^{\frac{V}{V_t}} - 1\right)$, we get (3.24) where $\zeta = 0.8, \lambda_1 = n_1\pi/(a_x + \Delta_x), \lambda_2 = n_2\pi/(a_y + \Delta_y)$

$$\begin{aligned} {F_{3\text{-}D}}^{-1} &= \frac{a_x}{(a_x + \Delta_x)}\frac{a_y}{(a_y + \Delta_y)} + \\ &\frac{2a_y}{(a_y + \Delta_y)}\sum_{n_1=1}^{\infty}\frac{\sin(\lambda_1 a_x)\cos(\lambda_1 x)}{n_1\pi\left(\sqrt{(\lambda_1 L_p)^2 + 1}\right)}\tanh\left(\sqrt{(\lambda_1 L_p)^2 + 1}\frac{W}{L_p}\right)\coth\left(\frac{W}{L_p}\right) + \\ = \quad &\frac{2a_x}{(a_x + \Delta_x)}\sum_{n_2=1}^{\infty}\frac{\sin(\lambda_2 a_y)\cos(\lambda_2 y)}{n_2\pi\left(\sqrt{(\lambda_2 L_p)^2 + 1}\right)}\tanh\left(\sqrt{(\lambda_2 L_p)^2 + 1}\frac{W}{L_p}\right)\coth\left(\frac{W}{L_p}\right) + \\ &\sum_{n_1=1}^{\infty}\sum_{n_2=1}^{\infty}\frac{4sin(\lambda_1 a_x)\cos(\lambda_1 x)\sin(\lambda_2 a_y)\cos(\lambda_2 y)}{n_1 n_2 \pi^2\left(\sqrt{(\lambda_1 L_p)^2 + (\lambda_2 L_p)^2 + 1}\right)}\tanh\left(\sqrt{(\lambda_1 L_p)^2 + (\lambda_2 L_p)^2 + 1}\frac{W}{L_p}\right)\coth\left(\frac{W}{L_p}\right) \end{aligned} \tag{3.24}$$

To give a feel for the effect of Δ_x, Δ_y on the spreading factor $F_{3\text{-}D}$, Fig. 3.3 gives a 3-D plot of it as a function of Δ_x, Δ_y. It can be easily shown that $F_{3\text{-}D}$ (3.24)→$F_{2\text{-}D}$ [2] for a

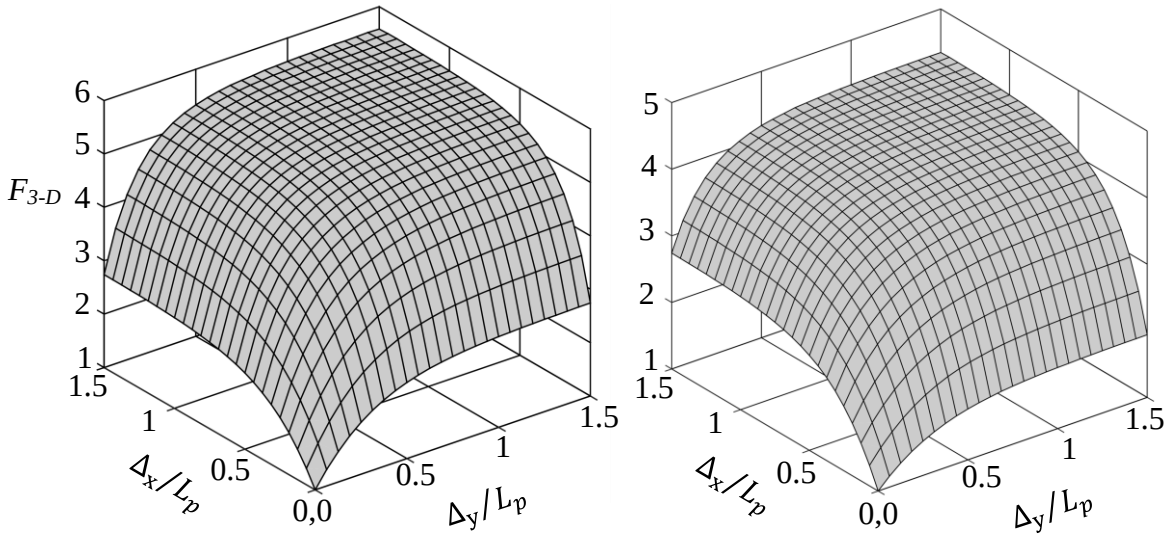

***Fig.* 3.3** DC or low frequency 3-D spreading factor in a 3-D plain with Δ_x, Δ_y as x and y coordinates and $F_{3\text{-}D}$ as z coordinate.

limiting case of Δ_x or Δ_y approaching zero. The forward DC current $\bar{I}$ can be obtained by integrating the current density $\bar{J}_{pz}$ over junction area. Since the current density is constant over the junction area, integration becomes simple multiplication and the current $\bar{I}$ is given as,

$$\bar{I} = 4a_x \times a_y \times \bar{J}_{pz} \tag{3.25}$$

3.2.2 Concentric junction with rounded corners

The 3-D mathematical analysis of a p-n junction with rectangular shaped p-region helped us gain a good understanding of the 3-D current spreading. We now use these results to understand the current spreading in a practical junction as given in Fig. 3.1(b).

The actual junction is replaced with a rectangular junction with sharp corners but having same area. The lateral extents a_x , a_y of the latter are a fraction f of the former and extent of n-region beyond the junction edge Δ_x , Δ_y are changed accordingly as

$$\begin{aligned} a_x = f(l_x/2 + r) \quad a_y = f\big(l_y/2 + r\big) \\ \Delta_x = \delta_x + (1-f)(l_x/2 + r) \\ \Delta_y = \delta_y + (1-f)\big(l_y/2 + r\big) \end{aligned} \tag{3.26}$$

where

$$f = \sqrt{1 - \frac{(4 - \pi)r^2}{(l_x + 2r)(l_y + 2r)}} \tag{3.27}$$

to match the areas of two junctions.

3.2.3 Eccentric Junction

Refer to Fig. 3.1(c). This geometry is separated into four quarters having currents I_{11}, I_{21}, I_{22}, I_{12} using two orthogonal vertical planes whose line of intersection passes through the center of the junction. The current in each quarter is approximated to be a quarter of the current through the corresponding symmetric structure, and the total current in the eccentric structure is derived as the sum of these four currents. This approach works for both sharp and rounded corners. Strictly speaking, the line of intersection of the planes of separation moves away from the centre of the junction as the junction is moved off-centre, as was found in the context of an eccentric spreading resistance [1]. However, we have found that for the case of forward biased diode studied here, this effect can be neglected without much loss of accuracy.

3.3 SOLUTION FOR THE SMALL-SIGNAL FORWARD CURRENT

This section discusses the analytical solution for small-signal excess hole distribution $\tilde{p}_e$ in the n-region, and small-signal hole current density $\tilde{j}_{pz}$ and current $\tilde{\imath}$ through the p-n junction. As stated in section (3.1), small-signal solutions are obtained by simply replacing L_p by L_p^* in the respective DC solutions

To get the small signal excess hole distribution, $\tilde{p}_e$ we replace L_p by L_p^* in (3.22). Next we relate $\tilde{p}_e$ to the small-signal voltage $\tilde{v}$ by the junction law, for obtaining a solution for $\tilde{j}_{pz}$ in terms of $\tilde{p}_e$. By law of the junction, the total hole density p_e at a location $(\zeta a_x, \zeta a_y)$ on the junction can be written as

$$p_e(\zeta a_x, \zeta a_y, 0) = p_{n0}\left(e^{\frac{V+\tilde{v}}{V_t}} - 1\right) \tag{3.28}$$

Since $\tilde{v}$ is small, $e^{\tilde{v}/V_t} \approx \left(1 + \frac{\tilde{v}}{V_t}\right)$, so that

$$\tilde{p}_e\,(\zeta a_x, \zeta a_y, 0) = p_{n0}\left(e^{\frac{V}{V_t}}\right)\frac{\tilde{v}}{V_t} \tag{3.29}$$

Which can be substituted in expression for $\tilde{p}_e$ to obtain

$$\tilde{j}_{pz} = \frac{F^*_{3-D} q p_{n_0} D_p e^{V/V_t}}{L^*_p} \frac{v}{V_t} \tag{3.30}$$

where

$$\begin{aligned} F^*_{3-D}{}^{-1} = & \frac{a_x}{(a_x+\Delta_x)} \frac{a_y}{(a_y+\Delta_y)} + \\ & \frac{2a_y}{(a_y+\Delta_y)} \sum_{n_1=1}^{\infty} \frac{\sin(\lambda_1 a_x)\cos(\lambda_1 x)}{n_1 \pi \left(\sqrt{(\lambda_1 L^*_p)^2+1}\right)} \tanh\left(\sqrt{(\lambda_1 L^*_p)^2+1}\frac{W}{L^*_p}\right) \coth\left(\frac{W}{L^*_p}\right) + \\ = & \frac{2a_x}{(a_x+\Delta_x)} \sum_{n_2=1}^{\infty} \frac{\sin(\lambda_2 a_y)\cos(\lambda_2 y)}{n_2 \pi \left(\sqrt{(\lambda_2 L^*_p)^2+1}\right)} \tanh\left(\sqrt{(\lambda_2 L^*_p)^2+1}\frac{W}{L^*_p}\right) \coth\left(\frac{W}{L^*_p}\right) + \\ & \sum_{n_1=1}^{\infty}\sum_{n_2=1}^{\infty} \frac{4sin(\lambda_1 a_x)\cos(\lambda_1 x)\sin(\lambda_2 a_y)\cos(\lambda_2 y)}{n_1 n_2 \pi^2 \left(\sqrt{(\lambda_1 L^*_p)^2+(\lambda_2 L^*_p)^2+1}\right)} \tanh\left(\sqrt{(\lambda_1 L^*_p)^2+(\lambda_2 L^*_p)^2+1}\frac{W}{L^*_p}\right) \coth\left(\frac{W}{L^*_p}\right) \end{aligned} \tag{3.31}$$

and

$$\tilde{\imath} = \tilde{j}_{pz} \times (4a_x a_y). \tag{3.32}$$

Same expression can be used for concentric and eccentric junction with rounded corners by doing similar modifications as in DC case.

3.4 SMALL-SIGNAL ADMITTANCE MODEL

In this section, we describe the models of the elements of the diode small-signal equivalent circuit reviewed in subsection 2.3.2.

3.4.1 Diffusion conductance and diffusion capacitance

Same as [2] we can write y_{dif} as ratio of small signal current, $\tilde{\imath}$ to small signal voltage $\tilde{v}$ and G_{diff}, C_{diff} as follows

$$y_{diff} = \frac{\tilde{\imath}}{\tilde{v}} \quad G_{diff} = Re(y_{diff}) \quad C_{diff} = \frac{Im(y_{diff})}{\omega} \tag{3.33}$$

where ω is the frequency in rad/s. Each of G_{diff} and C_{diff} can be separated into two parallel parts: a hole part G_{pdiff}, C_{pdiff} related to the n-region and an electron part G_{ndiff}, C_{ndiff} related to the p-region. G_{ndiff} and C_{ndiff} are expressed using the 1-D formulae available already (e.g. see [9]). We focus on G_{pdiff} and G_{pdiff} which are

influenced by current spreading effect.

We know that $Y_{pdiff} = G_{pdiff} + j\omega C_{pdiff}$. We can write $\tilde{j}_{pz}$ as $\tilde{v}/V_t$ times $\bar{J}_{pz}$ (e.g. see [9]) given by

$$\bar{J}_{pz} = F\left[\frac{qD_p}{L_p}\, p_{n0}\left(e^{\frac{V}{V_t}} - 1\right)\right]\coth\left(\frac{W}{L_p}\right) \tag{3.34}$$

with F/L_p replaced by F^*/L_p^* where F^* is $F_{3\text{-}D}^*$ given by (3.31), so that

$$Y_{pdiff} = F^*\sqrt{(1+j\omega\tau_p)}\left[\frac{qD_p}{L_p^*}\,\frac{p_{n0}\left(e^{V/Vt}\right)}{V_t}\right]\coth\left(\frac{W}{L_p^*}\right) \tag{3.35}$$

$$G_{pdiff} = \mathrm{Re}\left(F^*\sqrt{(1+j\omega\tau_p)}\left[\frac{qD_p}{L_p^*}\,\frac{p_{n0}\left(e^{V/Vt}\right)}{V_t}\right]\coth\left(\frac{W}{L_p^*}\right)\right) \tag{3.36}$$

$$C_{pdiff} = \mathrm{Im}\left(\frac{F^*\sqrt{(1+j\omega\tau_p)}}{\omega}\left[\frac{qD_p}{L_p^*}\,\frac{p_{n0}\left(e^{V/Vt}\right)}{V_t}\right]\coth\left(\frac{W}{L_p^*}\right)\right) \tag{3.37}$$

3.4.2 Transition capacitance

Conventional formula for depletion capacitance is based on the assumption that space-charge region is completely depleted of mobile carriers. But for a highly asymmetric junction like ours this condition fails as the lightly doped side gets inverted resulting in

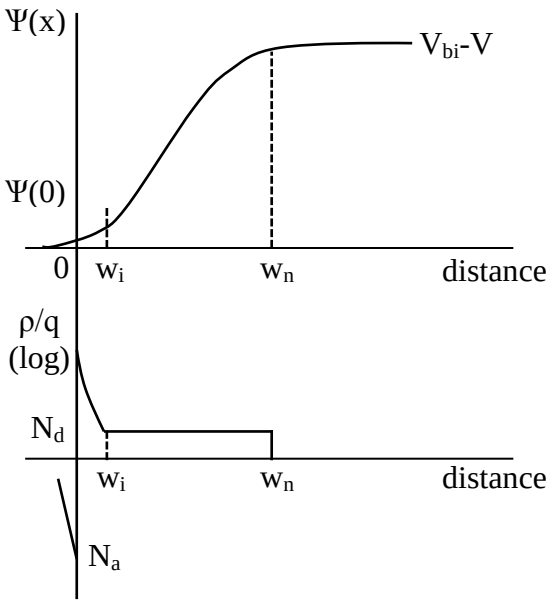

Fig. 3.4 Space-charge and potential distributions in an asymmetric junction

high concentration of minority carriers in space charge region next to the junction as shown in Fig. 3.4. This reduces the space charge layer width and thus changing the capacitance values. A closed form expression to account for this change has been given in [8] as

$$C_t = \sqrt{\frac{q\varepsilon_s N_d}{2\,[V_{bi} - V + V_t \ln(N_d/N_a)]}} + \alpha\left(\frac{1}{\sqrt{C_1^2 + \frac{N_d}{N_a}}} - \frac{w_i}{\sqrt{2}L_D} - \frac{\psi(0)}{V_t\sqrt{C_1^2 + e^{-\psi(0)/Vt}}}\right) \tag{3.38}$$

where the first term on the RHS is the classical expression for the depletion capacitance and the second term is the correction due to the presence of minority carriers in the space charge region. Further, α and C_1 are constants, w_i is the width of the inversion layer, L_D is the extrinsic Debye length in the n-region, $\psi(0)$ is the potential at the metallurgical junction. Same expression was used in [2] to find the depletion capacitance.

$$\alpha = \left[\frac{1}{V_t}\left(\frac{n_i}{C_1}\right)^2\sqrt{\frac{\varepsilon_s kT}{2N_a}}\left(e^{\frac{V}{V_t}} + \left({}^{N_d}/_{n_i}\right)^2\right)\right]\Big/(N_d + N_a) \qquad L_D = \sqrt{\frac{\varepsilon_s\, V_t}{qN_a}}$$

$$C_1 = \sqrt{\frac{\psi(0)}{V_t} - 1} \quad \psi(0) = \left[N_a V_t\left(1 - e^{\frac{-(V_{bi}-V)}{V_t}}\right) + N_d(V_{bi} - V)\right]\Big/(N_d + N_a) \tag{3.39}$$

$$w_i = \sqrt{2}L_D\left[\frac{\text{csch}^{-1}\left(\sqrt{N_d/N_a C_1^2}\right)}{C_1} - C_2\right] \quad C_2 = \text{csch}^{-1}\left(\sqrt{e^{-\psi(0)/V_t}/{C_1}^2}\right)/C_1$$

3.4.3 Bulk conductance and capacitance

Majority carrier drift current has been modelled extensively in literature in form of spreading resistance. As mentioned in [2] this DC model can be employed up to the frequency for which the skin depth $\sqrt{1/\pi f \mu\sigma}$ in the n-region remains much larger than its lateral dimension ($a + \Delta$). Using the same assumption we find G_s using the spreading resistance formulae for rectangular and square geometries given in the last row of Table I and Table II of [1]. Then we obtained $C_s = G_s\tau_d$, where τ_d = resistivity times the dielectric permittivity. For ease of reference, we reproduce below the spreading resistance formulae

of [1] used in our work.

For the rectangular geometry, the spreading resistance normalized to $R_{1D} = \rho W/(2a_x \times 2a_y)$ is given as

$$\begin{gathered}
\frac{R_{3\text{-}D}}{R^{\Delta_x}_{\Delta_y=0}} = (1-\gamma_1)\left[1+\frac{\Delta_y}{a_y}\right]^{\frac{\beta}{1-\gamma_1}} + \gamma_1, \quad \gamma_1 = \frac{R^{\Delta_x}_{\Delta_y\to\infty}}{R^{\Delta_x}_{\Delta_y=0}}, \quad \beta = -1 \\
\frac{R^{\Delta_x}_{\Delta_y=0}}{R_0} = (1-\gamma_2)\left[1+\frac{\Delta_x}{a_x}\right]^{\frac{\beta}{1-\gamma_2}} + \gamma_2, \ \gamma_2 = \frac{a_x}{2W\tan(\alpha_x)}\ln\left(1+\frac{2W\tan(\alpha_x)}{a_x}\right) \\
\frac{R^{\Delta_x}_{\Delta_y\to\infty}}{R^{\Delta_x=0}_{\Delta_y\to\infty}} = (1-\gamma_3)\left[1+\frac{\Delta_x}{a_x}\right]^{\frac{\beta}{1-\gamma_3}} + \gamma_3, \quad \gamma_3 = \frac{R^{\Delta_x\to\infty}_{\Delta_y\to\infty}}{R^{\Delta_x=0}_{\Delta_y\to\infty}} \\
\frac{R^{\Delta_x=0}_{\Delta_y\to\infty}}{R_{1\text{-D}}} = \frac{a_y}{2W\tan(\alpha_y)}\ln\left(1+\frac{2W\tan(\alpha_y)}{a_y}\right) \\
\alpha_y \approx \frac{53^\circ}{1+0.175(y/W)}, \quad \alpha_x \approx \frac{53^\circ}{1+0.175(x/W)} \\
\frac{R^{\Delta_x\to\infty}_{\Delta_y\to\infty}}{R_{1\text{-D}}} = \frac{1}{2W(\tan(\alpha_y)/a_y - \tan(\alpha_x)/a_x)}\ln\left[\frac{1+2W\tan(\alpha_y)/a_y}{1+2W\tan(\alpha_x)/a_x}\right]
\end{gathered} \tag{3.40}$$

for a long n-region, e.g. for $W = 5L_p$, and for a short n-region, e.g. for $W = 0.2L_p$ power law decay $[1+\Delta_x/a_x]^{\beta/(1-\gamma_{2,3})}$ and $\left[1+\Delta_y/a_y\right]^{\beta/(1-\gamma_1)}$ are replaced by the exponential decay $\exp\left[\frac{\beta}{1-\gamma_{2,3}}\left(\frac{\Delta_x}{x}\right)\right]$ and $\exp\left[\frac{\beta}{1-\gamma_1}\left(\frac{\Delta_y}{y}\right)\right]$respectively, with $\beta = 0.85$ and $\alpha_y = \alpha_x = 48°$.

Similarly, for the square geometry, the spreading resistance normalized to $R_{1\text{-}D} = \rho W/4a^2$ is given by the following relations.

$$\begin{gathered}
\frac{R_{3\text{-}D}}{R_{1\text{-}D}} = (1-\gamma)\left[1-\frac{\Delta}{a}\right]^{\frac{\beta}{1-\gamma}} + \gamma \\
\gamma = \frac{1}{1+(2W/a)\tan\alpha}, \beta = -2 \text{ and } \alpha = \frac{50}{1+0.175(a/W)}
\end{gathered} \tag{3.41}$$

for a long n-region, e.g. for $W = 5L_p$, and for small n-region, e.g. for $W = 0.2L_p$ the power law term $\left[1-\frac{\Delta}{a}\right]^{\frac{\beta}{1-\gamma}}$ is replaced by the exponential term $\exp\left[\frac{\beta}{1-\gamma}\left(\frac{\Delta_a}{a}\right)\right]$ and $\beta = -0.85, \alpha = 48°$

TABLE I

PARAMETERS OF THE P-N JUNCTION EMPLOYED IN CALCULATIONS

Parameter	p-side	n-side
Doping	N_a = 1 x 10^{18} cm^{-3}	N_d = 1 x 10^{16} cm^{-3}
Lifetime	τ_n = 10 ns	τ_p = 0.5 μs
Mobility	μ_n = 272.4 cm^2/ V-s	μ_n = 1122 cm^2/ V-s
	μ_p = 162.7 cm^2/ V-s	μ_p = 433.5 cm^2/ V-s
	L_n = 2.65 μm	L_p = 24 μm

3.5 MODEL VALIDATION AND DISCUSSION

3.5.1 Numerical Simulation set-up

Our model is validated by comparison with numerical calculations based on Sentaurus TCAD simulator [10] which employs mixed-boundary condition over the top surface, the drift-diffusion transport model with doping dependent lifetime and mobility, and electrostatic equations. 3-D simulations for the rectangular geometry were done for various lengths and breadths of devices and were compared with 1-D simulation for same lengths and breaths. Exploiting the symmetry of the device, only quarter of the device structure has been simulated. Meshing was designed in such a way that irrespective of device dimensions, number of mesh points was ~75000. The TCAD tool was calibrated by comparing the currents with analytical formulae available for 1-D and 2-D device [2].

As the equations are derived for holes in n-region by assuming p-region and depletion region as a 2-D disk, we need to match the results with hole current at depletion edge in n-region. To extract the same, the fact that p-region is shallow is exploited. Fig. 3.5 shows the variation of current in the device simulated and it is clear that due to the shallow junction and zero recombination in depletion region approximation, hole current at p-contact doesn't change till the depletion edge and can be used to match the results.

The model results are illustrated using a typical p^+-n silicon junction with junction depth of 0.2 μm, T = 300 K and other parameter values listed in Table I. The device has lateral dimensions of $0.2L_p \leq a_x, a_y \leq 5L_p$ and Δ_x, Δ_y in range of $0.2L_p$ to $1.5L_p$ and vertical dimensions of $0.2L_p \leq W \leq 5L_p$, where L_p = 24 μm. Small signal results are shown

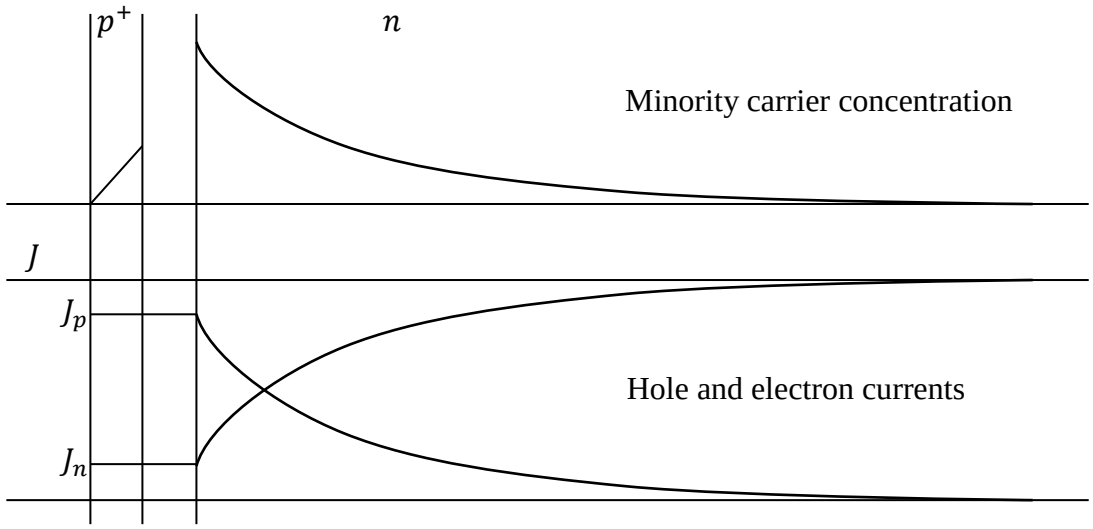

Fig. 3.5 Minority carrier concentration and hole and electron current density in shallow p-n junction.

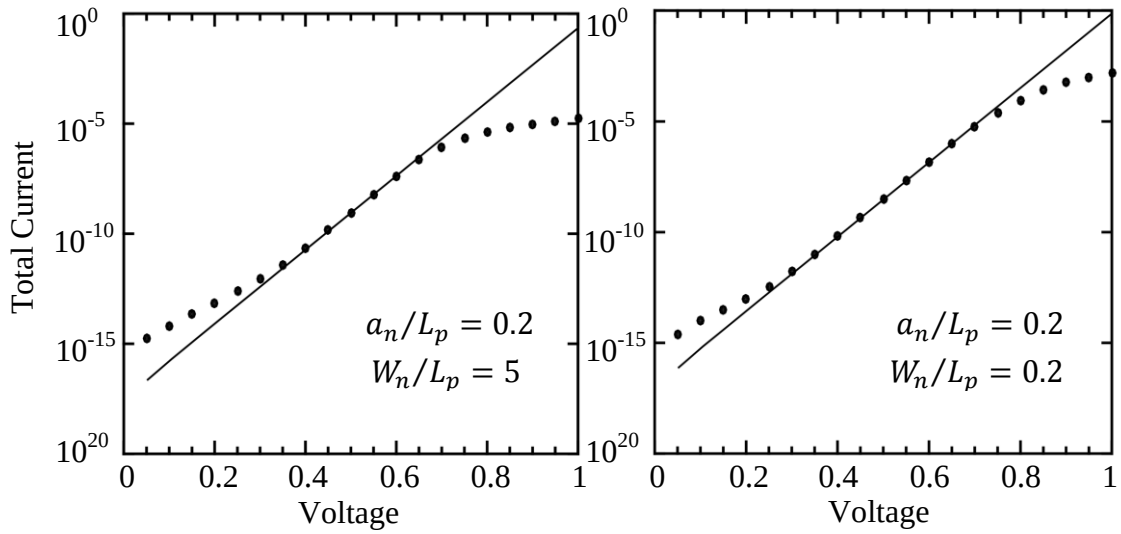

Fig. 3.6 Comparison of the simulated I-V data (dots) and the ideal diode model (line)

upto a frequency of 100 GHz which is close to the dielectric relaxation frequency of $1/2\pi\tau_d$ **(**τ_d = 0.6 ps). As discussed in section 3.4.3 given results work up to the frequency for which skin depth is much larger than the lateral dimensions of device. It was observed that at this 100 GHz, the skin depth in the p-region above the junction is about 3.5-7 times its lateral dimensions a_x,a_y. Hence, even after some reduction due to the much smaller skin depth in the metal above the p-region, the effective skin depth in the p-region [11] remains a few times a_x=a_y. Thus, our uniform current density boundary condition over a_x=a_y, and hence, our models for minority carrier current spreading, G_{dif} and C_{dif} remain valid upto this frequency. Similarly, the skin depth in the n-region is about 5-7 times its

lateral dimension ($a_x + \Delta_x$) = ($a_y + \Delta_y$). Hence, our models for majority carrier current spreading, G_s and C_s too are valid.

Ideal diode model is assumed to be valid in an applied bias range of 0.35- 0.6 V which can also be seen in Fig. 3.6. Thus we have performed our simulations at an applied bias of 0.5 V at which, the depletion layer recombination current is negligible compared to the diffusion current, yet low level injection prevails.

3.5.2 Results

First step to verify any results is to check the limiting cases. Limiting case for a rectangle as mentioned in section 3.2.1 will be when it becomes a stripe that is one of Δ_x or Δ_y goes to zero. Fig. 3.7 shows $F_{3\text{-}D}$ for such cases along with the $F_{2\text{-}D}$ from [2].

3.5.2.1 Concentric Junction with Sharp Corners

Fig. 3.8 shows the low frequency DC spreading factor $F_{3\text{-}D}$(3.24) as a function of W, Δ_x, Δ_y, a_x and a_y for a concentric structure. Similar to [2] the current spreading increases with W as well as Δ_x, Δ_y. For a given W, $F_{3\text{-}D}$ saturate for $\Delta > W$ in diodes with $W < L_p$ and for $\Delta > 1.2L_p$ in diodes with $W > 3L_p$. Our analytical calculations show that using $\zeta = 0.8$, $F_{3\text{-}D}$ matches with the numerical calculations within 7%. The simulations were done for an applied voltage of 0.5 V.

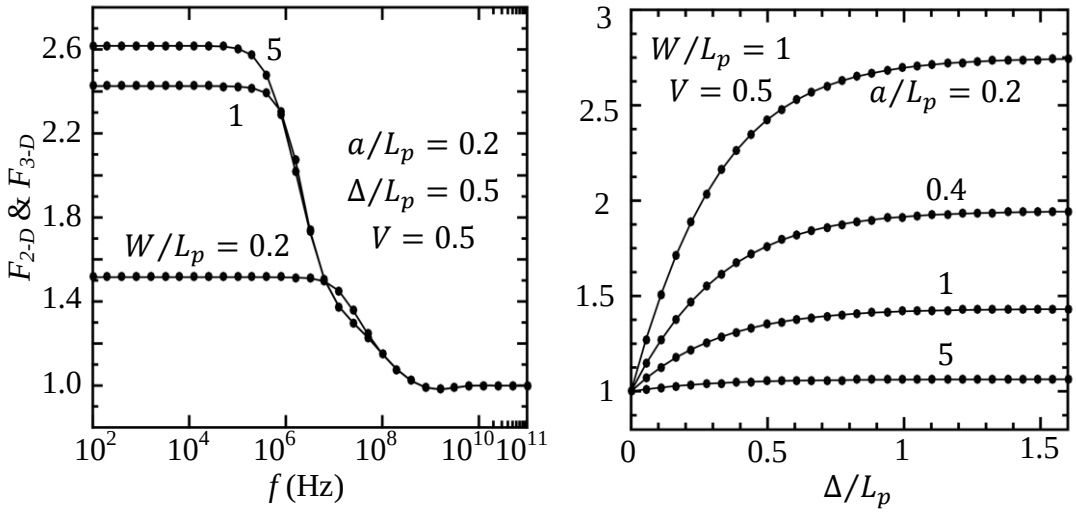

Fig. 3.7 DC or low frequency 2-D and 3-D spreading factors as a function of device geometry. Continuous lines show our model, points show model given by *[2]*.

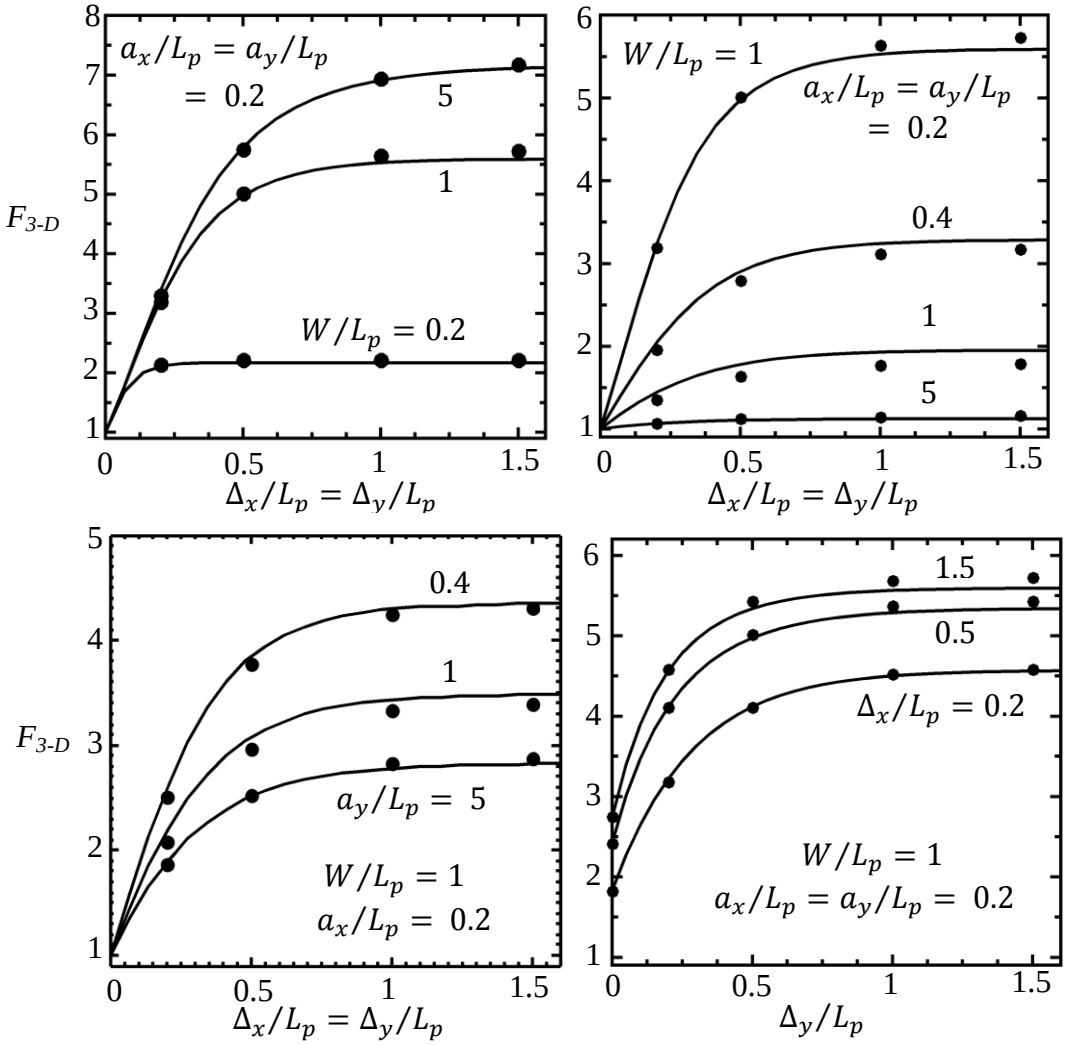

Fig. 3.8 DC or low frequency 3-D spreading factor as a function of device geometry. Continuous lines show model and points show simulations .

Our extensive calculations show that, for a given *W*, the values of Δ_x or Δ_y at which the DC spreading saturates fit into the empirical relation

$$\Delta_{sat} = 1.2 \tanh(W/L_p) \tag{3.42}$$

which also applies to stripe and circular geometries in [2]. The current spreading factor decreases as a_x or a_y increases i.e. as the junction area increases, the current can be safely assumed to be almost 1-D since the contribution of the lateral current component becomes negligible as compared to the vertical current component.

The magnitude of small-signal minority carrier current spreading factor $F^*_{3\text{-}D}$ (3.31) of a concentric square junction with $a_x = a_y = 0.2L_p$ and $\Delta_x = \Delta_y = 0.5L_p$ is shown in Fig. 3.9.

It can be seen that minority carrier current spreading gets restricted with increasing frequency. It falls-off for $f > 1/2\pi\tau_p$ in long diodes ($W \geq 3L_p$) and for $f > 1/2\pi\tau_t$ in short diodes ($W \leq 0.2L_p$), and finally saturates to 1; here, $\tau_t = W^2/2\text{-}D_p$ is the transit time (10 ns for $W = 0.2L_p$). This means that at high frequencies, minority carrier flow picture is such that we have 1-D small signal flow superimposed over 3-D DC flow.

Next we discuss the small signal model of the concentric junction. Unlike DC case the simulator doesn't give terminal current for the AC case. It gives only capacitance and conductance of the junction and hence we have validated our model as per the equivalent circuit shown in Fig. 2.7, where G_{dif}, G_s are the diffusion, series conductance and C_{dif}, C_{dep}, $C_s = G_s\tau_d$ are the diffusion, depletion, dielectric relaxation capacitance, all per unit area of the 1-D junction.

Fig. 3.10 compares our analytical calculations for the small-signal conductance and capacitance with numerical calculations over a wide frequency range of 100 Hz – 100 GHz for long and short diodes. A forward bias of 0.35 and 0.6 V is employed so that the whole range voltage where ideal diode model is applicable is considered. The analytical results are within 20 % of the numerical results. The conductance = G_{dif} and capacitance = $C_{dif} + C_{dep}$ are independent of frequency for $f < 1/2\pi\tau_p$ for long diodes and $f < 1/2\pi\tau_t$ for short diodes. As frequency is raised, the conductance rises while the capacitance falls, ultimately saturating at G_s and C_s respectively.

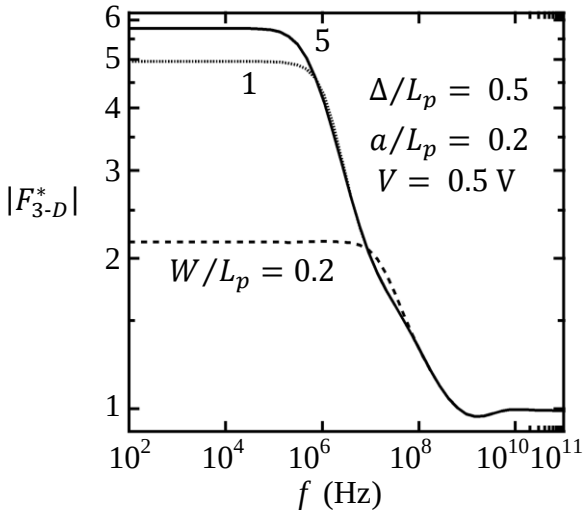

***Fig.* 3.9** Small signal 3-D spreading factors for minority carrier current as a function of frequency.

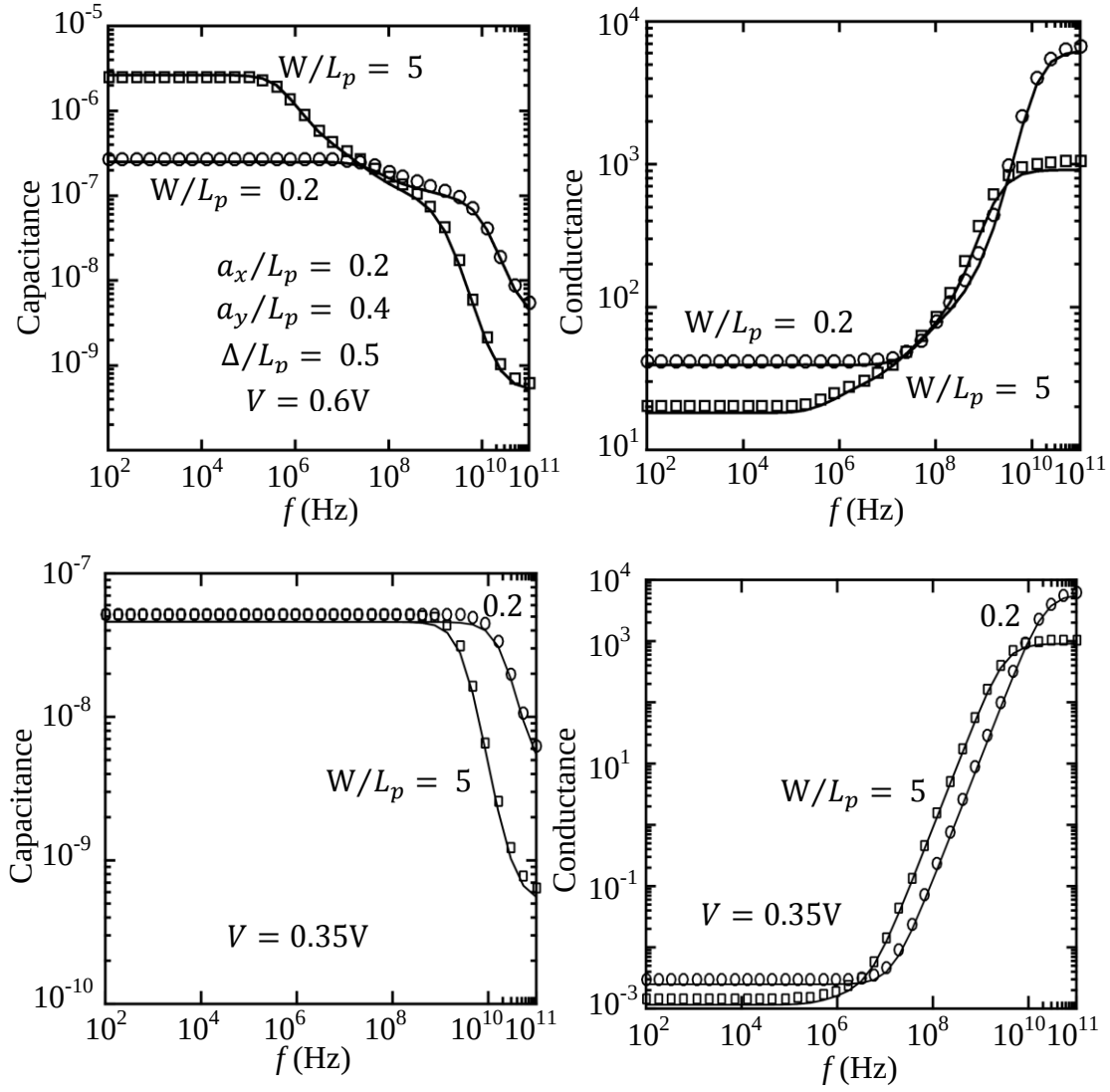

***Fig.* 3.10** Conductance and capacitance of rectangular junction as a function of frequency, for long (W/L_p = 5) and short (W/L_p = 0.2) diodes. Continuous lines show model and symbols show simulations. Here the applied voltage is 0.35 and 0.6 V.

3.5.2.2 Concentric Junction with rounded corners

Table II compares the model calculations using (3.24)-(3.27) with TCAD calculations for a variety of geometries. The difference between the two calculations is < 5%. The worst case occurs when the junction is circular and the semiconductor area is square, i.e. in Fig. 3.1(b), $l_x = l_y = 0$ and $\delta_x = \delta_y$.

3.5.2.3 Eccentric Junction

Fig. 3.11 shows the variation of $F_{3\text{-}D}$ in an eccentric junction as the junction is moved around over the n-region. Results of our analytical model discussed in section 3.2.3 match

TABLE II

COMPARISON OF PRESENT MODEL WITH TCAD; $W/L_P = 1$

$\frac{l_x}{L_p}$	$\frac{l_y}{L_p}$	$\frac{r}{L_p}$	$\frac{\delta_x}{L_p}$	$\frac{\delta_y}{L_p}$	$F_{3\text{-}D}$		% Error
					TCAD	Model	
0	0	0.2	0.5	0.5	5.64	5.59	-0.75
		0.2	1.0	1.0	6.29	6.13	-2.60
		0.4	0.5	0.5	3.11	3.23	3.97
		0.4	1.0	1.0	3.39	3.54	4.19
0.1	0.1	0.1	0.5	0.5	5.17	5.11	-1.20
		0.3	0.5	0.5	2.96	3.07	3.88
0.2	0.2	0.2	0.5	0.5	2.90	2.97	2.38
0.3	0.3	0.1	0.5	0.5	2.87	2.92	1.76
0.2	0.0	0.2	0.2	0.4	3.40	3.39	-0.43
0.3	0.1	0.1	0.2	0.4	3.24	3.22	-0.58

with the TCAD simulations within 7% error.

3.6 COMPARISON

In this section we compare our model with 2-D approximation and also discuss some approximations which expand the scope of our model for geometries other than rectangular.

3.6.1 Practical Junction

In section 3.2.2 we provided a method to find the current spreading in a concentric junction with rounded corners. Another method to calculate same was outlined in [2] using the formulas for stripe and circular geometries. It considered spreading as a combination of 2-D effect along the edges and 3-D effects at the corners. The method is briefly described here for ease of reference. Consider the junction given in LHS of Fig. 3.12 and separate the junction area into stripes ABCD and EFGH, and four quarter circles1, 2, 3, and 4, which can be combined to form a circular junction. The stripe ABCD has length = *l*, width $2a_x = (w+2r)$, and lateral extension Δ_x = [AB-(*w*+2*r*)]/2; stripe EFGH has length = *w*, $2a_y$ = (l+2*r*), and Δ_y = [EF-(l+2*r*)]/2; the circular junction has a radius *a* = *r*, and its lateral extension has an upper limit = *U* and lower limit = *L* , which is the smaller of the lateral extensions of the two stripes. The current *I* through the junction

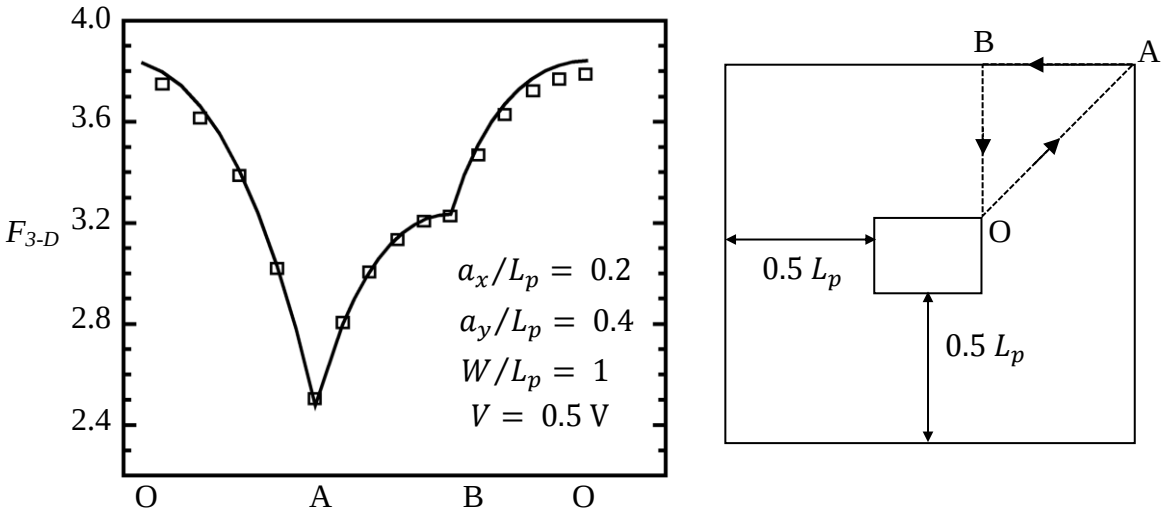

Fig. 3.11 DC or low frequency 3-D spreading factor for eccentric rectangular junction obtained by moving the junction along the path OABO.

is the sum of the 1-D current through the junction area, 2-D spreading from the two stripes, and 3-D spreading from the circle.

Let F_{ABCD} and F_{EFGH} denote the 2-D spreading factors associated with the stripes and F_{1234} denotes the 3-D spreading factor associated with the circle; estimated using (6) and (7) in [2] then

$$I = [(F_{ABCD} - 1)l(w + 2r) + (F_{EFGH} - 1)w(l + 2r) + F_{1234}\pi r^2 + wl + 2r(w + l)]J_{1\text{-}D} \tag{3.43}$$

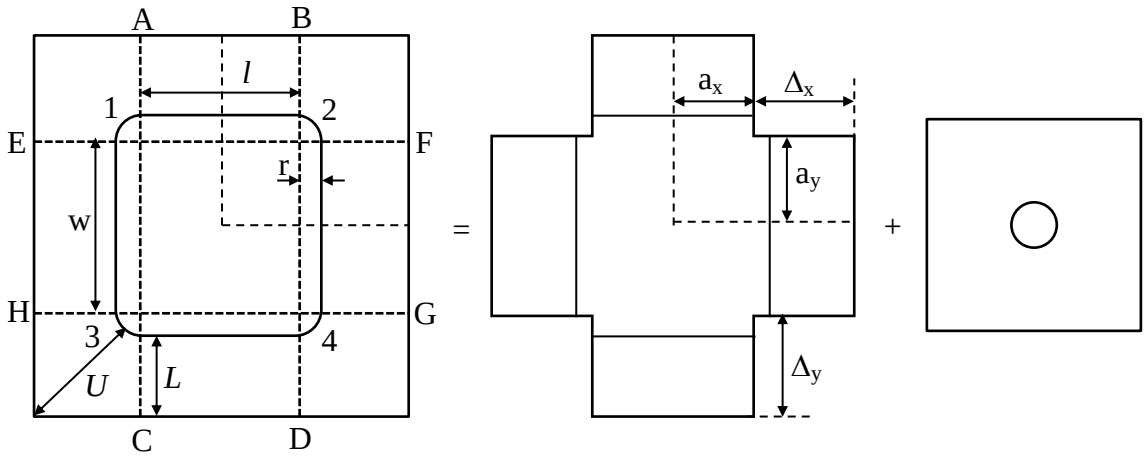

Fig. 3.12 Method to simplify a practical junction as suggested in [2]

TABLE III

Comparison of 1-D, 2-D and 3-D model with TCAD; $\Delta_x/L_p = \Delta_y/L_p = 1.5$

a_x	a_y	W	3-D Simulated Current (nA)	1-D Model		2-D Model		3-D Model	
				Current (nA)	Error	Current (nA)	Error	Current (nA)	Error
0.2		0.2	6.42	2.95	54%	5.61	13%	5.92	8%
		1	4.34	1.07	75%	3.39	22%	4.09	6%
		5	4.24	0.91	78%	3.19	25%	3.98	6%
0.4		0.2	18.7	11.8	37%	17.6	6%	17.9	4%
		1	10.3	4.22	59%	9.21	11%	10.2	1%
		5	9.89	3.59	64%	8.53	14%	9.74	2%
1		0.2	93	73.2	21%	84.7	9%	84.6	9%
		1	40.9	26.1	36%	40.3	1%	41.8	-2%
		5	37.6	22.2	41%	36.1	4%	38.0	-1%

Table III shows the comparison between two approaches along with the 1-D model. In these calculations the radius of the junction corner was assumed to be equal to the junction depth of 0.2 μm, $\Delta_x = \Delta_y = 1.5L_p$, $W/L_p = 1$ and other parameters were as in Table I. We found that, the results of [2] deviate from TCAD results by as much as 25% for $a_x = a_y = 0.2L_p$, i.e. when the junction approaches a square shape and its size is less than diffusion length; under these conditions, the current spreading from the corners is significant, which is not captured by the approach of [2] i.e. it only considers the spreading in the devices given in the R.H.S of Fig. 3.12. The circular region considered has a very small radius and has negligible effect on total current. However, for the same conditions, results of the approach deviate by $\leq$ 9%, demonstrating the ability of the present approach to accurately model the spreading from corners. An important observation is that beyond a_x, $a_y = L_p$ results are almost same for 2-D and 3-D models which means that beyond $a_x, a_y \geq L_p$, 3-D spreading in corners becomes insignificant as compared to the spreading in the edges.

3.6.2 Non-Rectangular Geometries

Fig. 3.13(a) compares the $F_{3\text{-}D}$ predictions of a square junction with those of a circular junction with same area, based on TCAD, and (3.24) for a rectangular junction and (7) of [2] for a circular junction. The TCAD simulations of the square and circular junctions are within 2% of each other and hence represented by a single set of points. The maximum

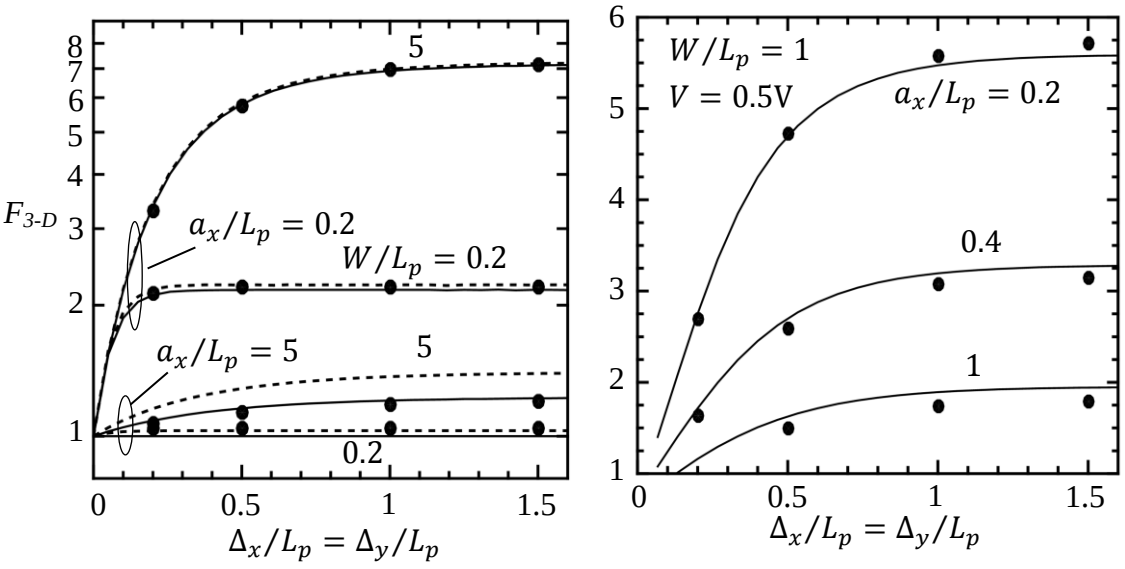

Fig. 3.13 (a) Comparison between models for circular (dashed lines) and square (solid lines) junctions of same area. TCAD simulations of both junctions are identical and shown by points. (b) Comparison between model for square (solid lines) and TCAD simulations (points) for a square p-region on a circular n-region. Here Δ represents difference between radius of circle and half the side of square.

difference between the two models is 14%, which occurs for large junction areas; for small junctions, the difference is much less. It should be noted that present model matches the simulations for all scenarios. We already showed in section 3.2.2 how the results for circle in a square could be predicted using $F_{3\text{-}D}$ and here we show that a circle in circle can also be approximated as a square in square of equal area. The possibility of whether a square in a circle can be predicted using the same approach was also verified as shown in Fig. 3.13(b). These results along with results in [1] show that for device modelling purpose circular/elliptical and square/rectangular geometries are transposable.

As far as calculation time is concerned, it takes ~ 200 ms to calculate the zeroes of the Bessel's function in (7) of [2]. However, the zeroes can be calculated once for all, stored and reused for estimating $F_{3\text{-}D}$ of any circular junction; thereafter, the calculation time is ~ 2 ms. Time taken to calculate the $F_{3\text{-}D}$ of a square junction is about 6 ms. The utility of the analytical model for device design and circuit simulation is seen from the fact that the model calculations can be done using MATLAB and take on the order of milliseconds. In contrast, TCAD simulations can be carried out only with a high level of specialized training in the choice of mesh, physical models and solvers to obtain a convergent solution for the specific device structure and bias conditions at hand. Also, they take on

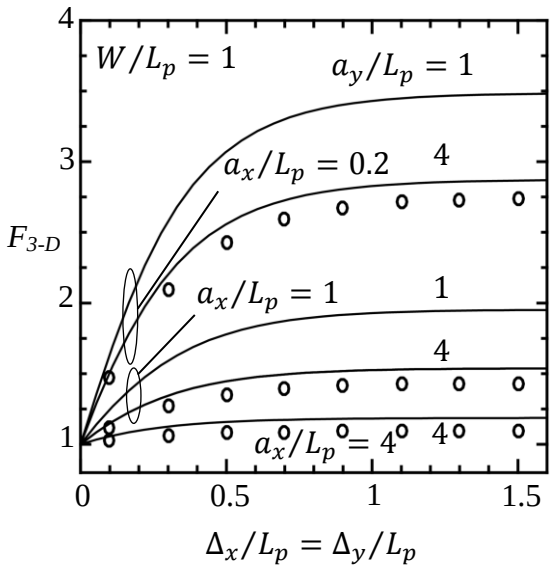

Fig. 3.14 Comparison between rectangular and stripe shaped junctions

the order of hundreds of seconds, which is four orders of magnitude higher than the time taken by the model. The above times correspond to an Intel i7 Octacore processor with 32 GB RAM.

Finally, we anticipate that, the current spreading in the direction of a side of the rectangle can be neglected if the dimension of this side exceeds a few diffusion lengths. This is brought out in Fig. 3.14, where we plot the spreading factor $F_{3\text{-}D}$ of a rectangular junction as a function of $\Delta_x = \Delta_y$, for a given a_x and W, and increasing a_y. The figure also includes the $F_{2\text{-}D}$ of a stripe shaped junction calculated using (6) of [1] for the same a_x and W. It is seen that the $F_{3\text{-}D}$ curve approaches the $F_{2\text{-}D}$ curve for $a_y/L_p > 4$.

Chap 4. MODEL FOR A JUNCTION WITH HI-LO BACK CONTACT

In previous chapter we discussed the current spreading in forward biased shallow p-n junction having a perfectly absorbing boundary at the bottom surface of n-region. This condition amounts to an ideal ohmic contact to the n-region. But practically one may encounter a case where n-region is followed by an n^+-film to improve the quality of contact, as shown in Fig. 4.1(a). Fig. 4.1(b) shows the difference in minority current value that arises due to this modification as compared to a p^+n junction. It is because for HI-LO junction the excess minority carrier concentration at the bottom boundary is not zero as in the case for an ohmic contact. This reduces the minority carrier gradient in the n-region which leads to a reduction in diffusion current. As the length of n-region is reduced the concentration at boundary further increases and thus reducing the current even more. This scenario is modelled in [12] by replacing the nn^+ junction with a boundary having an effective surface recombination velocity, *S*. The value of the effective recombination velocity is process dependent. We have assumed a variable *S* to derive our model.

4.1 DEVICE STRUCTURE, EQUATIONS, BOUNDARY CONDITIONS AND APPROXIMATIONS.

We use the device structure same as previous chapter with all the symbols meaning

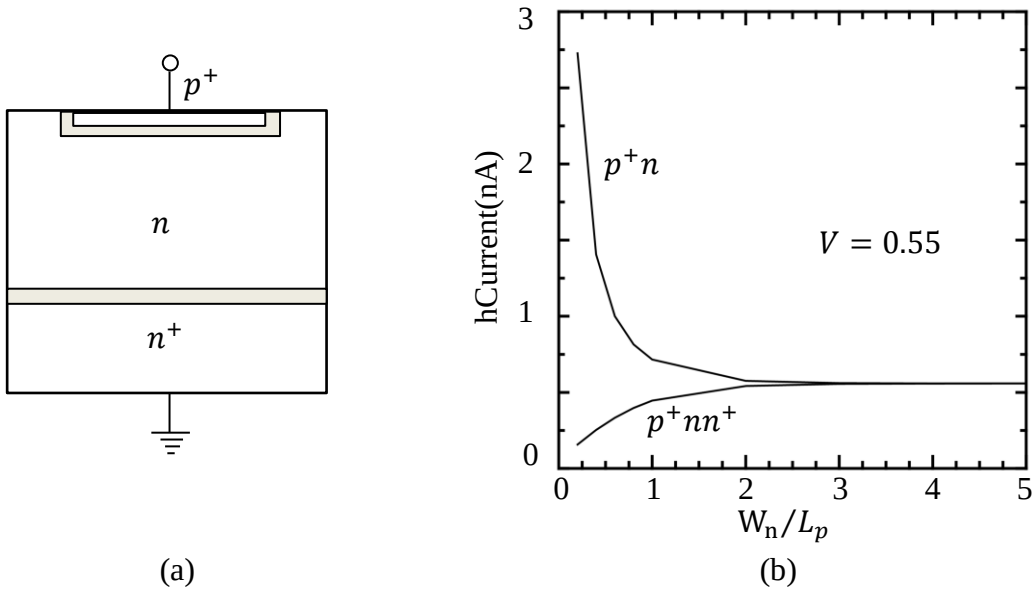

(a) (b)

Fig. 4.1 (a) p^+nn^+ junction (b) Comparison of hole current in p^+n junction with p^+nn^+junction (simulated).

same. We make same assumptions regarding device structure and device physics as made in previous chapter. Again we consider a quarter of the structure and minority carrier continuity equation (2.6) is solved with same boundary conditions as previous chapter except the boundary condition at the back contact which is given as

$$qD_p \frac{\partial p_e}{\partial z}\Big|_{z=W} + qSp_e(W) = 0 \Rightarrow \frac{\partial p_e}{\partial z}\Big|_{z=W} + \frac{\alpha p_e(W)}{L_p} = 0 \quad \text{where } \alpha = \frac{SL_p}{D_p} \tag{4.1}$$

If we keep $S \rightarrow \infty$ in above equation it will translate to $p_e(W) = 0$ as used in previous chapter.

4.2 SOLUTION FOR DC FORWARD CURRENT

We solve (2.6) in rectangular coordinate system using the method of separation of variables to write the solution as

$$p_e = X.Y.Z \quad \text{where } p_e(x) \rightarrow X, p_e(y) \rightarrow Y, p_e(z) \rightarrow Z \tag{4.2}$$

Solutions for X and Y remain the same and are reproduced here for convenience

$$X = B\cos(\lambda_1 x) \text{ where } \lambda_1 = \frac{n_1\pi}{a_x + \Delta_x} \text{ and } n_1 = 1,2,3,4.\ldots\infty \tag{4.3}$$

$$Y = C\cos(\lambda_2 y) \text{ where } \lambda_2 = \frac{n_2\pi}{a_y + \Delta_y} \text{ and } n_2 = 1,2,3,4.\ldots\infty \tag{4.4}$$

With new boundary conditions at $z=W$ the solution for Z becomes

$$Z = E\left(\frac{\alpha}{kL_p}\sinh\big(k(W-z)\big) + \cosh\big(k(W-z)\big)\right) \quad \text{where } k = \left(\sqrt{\lambda_1^2 + \lambda_2^2 + \frac{1}{L_p^2}}\right) \tag{4.5}$$

Thus we can write the general solution for $\boldsymbol{p_e}$ as the linear sum of all combinations of $X.Y.Z$ to obtain

$$p_e(x,y,z) = \sum_{n_1=0}^{\infty}\sum_{n_2=0}^{\infty} A_{n_1 n_2}\cos(\lambda_1 x)\cos(\lambda_2 y)\left(\frac{\alpha}{kL_p}\sinh\big(k(W-z)\big) + \cosh\big(k(W-z)\big)\right) \tag{4.6}$$

Next we apply the boundary condition at *z=0* and repeat the procedure used in section 3.2.1 to consider all the cases of n_1 and n_2 and get the final solution for excess hole concentration in n-region as

$$p_e(x,y,z) = A\frac{\alpha\sinh\left(\frac{W-z}{L_p}\right)+\cosh\left(\frac{W-z}{L_p}\right)}{\sinh\left(\frac{W}{L_p}\right)+\alpha\cosh\left(\frac{W}{L_p}\right)} + \sum_{n_1=1}^{\infty} A_{n_1}\cos(\lambda_1 x)\frac{\frac{\alpha}{k_1L_p}\sinh\big(k_1(W-z)\big)+\cosh\big(k_1(W-z)\big)}{\sinh(k_1W)+\frac{\alpha}{k_1L_p}\cosh(k_1W)} + \sum_{n_2=1}^{\infty} A_{n_2}\cos(\lambda_2 y)\frac{\frac{\alpha}{k_2L_p}\sinh\big(k_2(W-z)\big)+\cosh\big(k_2(W-z)\big)}{\sinh(k_2W)+\frac{\alpha}{k_2L_p}\cosh(k_2W)} + \sum_{n_1=1}^{\infty}\sum_{n_2=1}^{\infty} \mathrm{A_{n_1n_2}}\cos(\lambda_1 \mathrm{x})\cos(\lambda_2 y)\frac{\frac{\alpha}{k_{12}L_p}\sinh\big(k_{12}(W-z)\big)+\cosh\big(k_{12}(W-z)\big)}{\sinh(k_{12}W)+\frac{\alpha}{k_{12}L_p}\cosh(k_{12}W)} \tag{4.7}$$

Where

$$A = \frac{J_{p_z}}{qD_p/L_p}\frac{a_x}{(a_x+\Delta_x)}\frac{a_y}{(a_y+\Delta_y)}$$

$$A_{n_1} = \frac{a_y}{(a_y+\Delta_y)}\frac{\frac{2J_{p_z}}{qD_p/L_p}\sin(\lambda_1 a_x)}{n_1\pi\left(\sqrt{(\lambda_1 L_p)^2+1}\right)} \qquad k_1 = \sqrt{\lambda_1^2+\frac{1}{L_p^2}}$$

$$A_{n_2} = \frac{a_x}{(a_x+\Delta_x)}\frac{\frac{2J_{p_z}}{qD_p/L_p}\sin(\lambda_2 \mathrm{a_y})}{n_2\pi\left(\sqrt{(\lambda_2 \mathrm{L_p})^2+1}\right)} \qquad k_2 = \sqrt{\lambda_2^2+\frac{1}{L_p^2}}$$

$$A_{n_1n_2} = \frac{\frac{4J_{p_z}}{qD_p/L_p}\sin(\lambda_1 \mathrm{a_x})\sin(\lambda_2 \mathrm{a_y})}{n_1n_2\pi^2\left(\sqrt{(\lambda_1 L_p)^2+(\lambda_2 L_p)^2+1}\right)} \qquad k_{12} = \sqrt{\lambda_1^2+\lambda_2^2+\frac{1}{L_p^2}}$$

To solve for $\bar{J}_{pz}$ we relate $\bar{p}_e$ to applied voltage, *V* using junction law same as done in previous chapter and by using the same value of ζ. We express $\bar{J}_{pz}$ as a product of a current spreading factor $F_{3\text{-}D}$ and the current density under 1-D conditions i.e

$$\bar{J}_{pz} = F_{3\text{-}D}\frac{qD_p}{L_p}p_{n0}\left(e^{\frac{V}{V_t}}-1\right)\times \mathrm{K} \quad \text{where } K = \left(\frac{1+\alpha\coth\left(W/L_p\right)}{\alpha+\coth\left(W/L_p\right)}\right) \tag{4.8}$$

Where

$$\begin{aligned} & {F_{3\text{-}D}}^{-1} \\ & \frac{a_x}{a_x+\Delta_x}\frac{a_y}{a_y+\Delta_y}+ \\ & \frac{2a_y}{a_y+\Delta_y}\sum_{n_1=1}^{\infty}\frac{\sin(\lambda_1 a_x)\cos(\lambda_1 x)}{n_1\pi\sqrt{\left(\lambda_1 L_p\right)^2+1}}\left(\frac{\alpha/k_1L_p+\coth(k_1W)}{1+\alpha\coth(k_1W)/k_1L_p}\right)\times \mathrm{K} + \\ = & \frac{2a_x}{a_x+\Delta_x}\sum_{n_2=1}^{\infty}\frac{\sin\left(\lambda_2 a_y\right)\cos(\lambda_2 y)}{n_2\pi\sqrt{\left(\lambda_2 L_p\right)^2+1}}\left(\frac{\alpha/k_2L_p+\coth(k_2W)}{1+\alpha\coth(k_2W)/k_2L_p}\right)\times \mathrm{K} + \\ & \sum_{n_1=1}^{\infty}\sum_{n_2=1}^{\infty}\frac{\sin(\lambda_1 a_x)\cos(\lambda_1 x)\sin\left(\lambda_2 a_y\right)\cos(\lambda_2 y)}{n_1 n_2\pi\sqrt{\left(\lambda_2 L_p\right)^1+\left(\lambda_2 L_p\right)^2+1}}\left(\frac{\alpha/k_{12}L_p+\coth(k_{12}W)}{1+\alpha\coth(k_{12}W)/k_{12}L_p}\right)\times \mathrm{K} \end{aligned} \tag{4.9}$$

4.3 SMALL SIGNAL MODEL

To find small signal minority carrier current same methodology can be used as section 3.3 and (4.9) can be modified accordingly to obtain small signal frequency dependent spreading factor. For majority carriers as the current is due to drift and excess carrier concentration is negligible, change in boundary condition at bottom surface of n-region is expected to have no effect. This fact was also verified by TCAD simulations. Thus we can use the same model for majority carrier spreading as used in section 3.4.

4.4 MODEL VALIDATION AND DISCUSSION

4.4.1 Numerical Simulation Set-up

Our model is validated by comparison with numerical calculations based on Sentaurus TCAD simulator. 3-D simulations were done for rectangular geometries of various lengths and breadths of devices. The simulator allows us to specify carrier recombination velocity at contacts. This was used to specify hole recombination velocity at n-contact. It was also verified that changing boundary condition for electrons had no effect on current at all.

The TCAD tool was calibrated by simulating a 1-D p-n junction and comparing with the values calculated using analytical formulae as shown in Fig. 4.2.

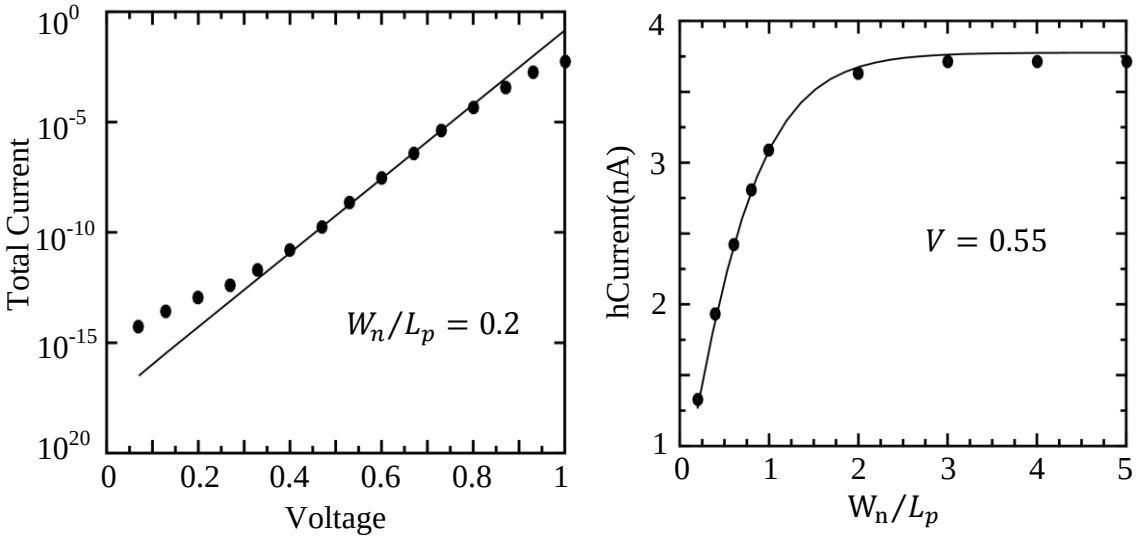

Fig. 4.2 Comparison of simulated I-V data (points) and ideal diode model (lines)

For the case of p^+nn^+ junction at applied bias of 0.5 V hole current for certain geometries drops to values comparable to recombination current in space-charge layer. This fails our method of extracting the hole current on depletion edge. Thus the simulations are performed at applied bias of 0.55 V, which ensures that recombination current is negligible and low level conditions prevail.

The model results are illustrated using a typical p^+-n silicon junction with junction depth of 0.2 μm, T = 300 K, hole recombination velocity, S = 700 cm/s on n-contact and other parameter values listed in Table I. The device has lateral dimensions of $0.2L_p \leq a_x, a_y \leq 5L_p$ and Δ_x, Δ_y in range of $0.2L_p$ to $1.5L_p$ and vertical dimensions of $0.2L_p \leq W \leq 5L_p$, where L_p = 24 μm.

4.4.2 Results and discussions

Fig.4.3 shows the low frequency or DC spreading factor $F_{3\text{-}D}$ as a function of W, Δ_x, Δ_y, a_x, a_y for a p^+n junction with hi lo back contact. Value of ζ is used same as the case of a p^+n junction with ohmic contacts. Our analytical calculations show that using ζ = 0.8, $F_{3\text{-}D}$ matches with the numerical calculations within 7%.

It can be observed that for a p^+n junction with hi lo back contact spreading increases with decrease in W_n which is opposite of what we observed in case of p^+n junction with ohmic back contact. It is because for this boundary condition the current decreases with decrease in W_n and the carriers contributing to 1-D current travel distance less than the

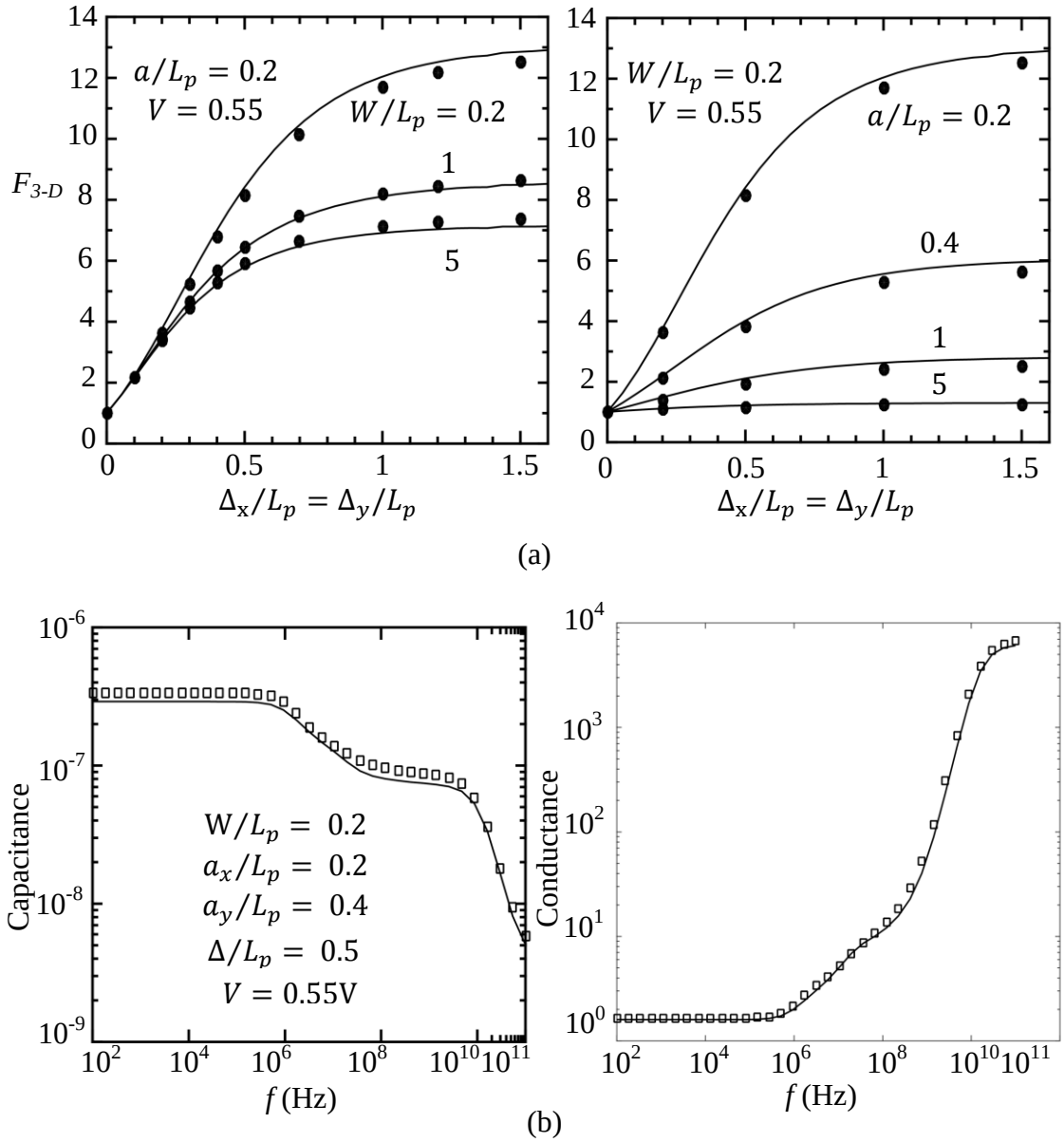

Fig. 4.3 (a) DC spreading factor as a function of device geometry **(b)** Conductance and capacitance of rectangular junction as a function of frequency for short (W/Lp = 0.2) diodes. Continuous lines show model and symbols show simulations.

carriers contributing in 2-D/3-D current. Thus the current contribution by laterally spread carriers is more than carriers travelling straight and this difference increases with decreasing width of n-region.

Fig. 4.4 compares the capacitance and conductance obtained from our analytical calculations with the TCAD simulations. Model for conductance shows a maximum error of about 14% and for conductance maximum error is about 24%. The results have been shown only for small diode as that is where the effect of boundary condition is evident.

Chap 5. CONCLUSIONS

We derived an analytical model for minority carrier current spreading, in forward biased shallow rectangular p-n junctions which could be eccentric and may have rounded corners. We showed that, under small-signal conditions, the spread of the minority carrier flow gets restricted for $f > 1/2\pi\tau_p$ in long diodes with $W > 3L_p$ and $f > 1/2\pi\tau_t$ for short diodes with $W < 0.2L_p$. The flow becomes almost 1-D at large frequencies. Under DC conditions, the minority carrier flow saturates for $\Delta > W$ in diodes with $W < L_p$ and for $\Delta > 1.2L_p$ in diodes with $W > 3L_p$; the flow is almost 1-D in short diodes with $W < 0.2L_p$ but spreads with increase in W, and saturates in long diodes with $W > 3L_p$. The spreading in a circular junction approximates that in a square junction of the same area, and that in the direction of a side $> 4L_p$ can be neglected. Next we modelled a general p^+nn^+ junction with arbitrary surface recombination velocity at the lower boundary of n-region. It was found that spreading increased with a decrease in length of n-region for a p^+nn^+ junction which is opposite to the case of p^+n junction. The model was validated by comparison with numerical simulation.

Future work can incorporate the current emanating from the vertical side walls of the junction that was neglected in our work. It can also attempt to achieve a semi-empirical formula for current spreading to replace the infine summation expressions derived in this report. One can also take a device with n^+ isolation walls i.e the vertical side-walls are also nn^+ and find spreading current for that case.

REFERENCES

[1] S. Karmalkar, P. V. Mohan, H. P. Nair and Y. Ramya, "Compact Models of Spreading Resistances for Electrical/Thermal Design of Devices and ICs," *IEEE Trans. Electron Devices,* vol. 54, no. 7, p. 1437, 2007.

[2] V. K. Gurugubelli, R. C. Thomas and S. Karmalkar, "An Analytical Model of the DC and Frequency-Dependent 2-D and 3-D Current Spreading in Forward-Biased Shallow p-n Junctions," *IEEE Trans. Electron Devices,* vol. 62, no. 2, pp. 471-477, 2014.

[3] C. A. Grimbergen, "The influence of geometry on the interpretation of the current in epitaxial diodes," *Solid-State Electronics,* vol. 19, no. 12, pp. 1033-1037, 1976.

[4] D. J. Roulston, M. H. Elsaid, M. Lau and L. A. Watt, "Corner Currents in Rectangular Diffused p+-n-n+ Diodes," *IEEE Trans. Electron Devices,* vol. 25, no. 3, pp. 392-393, 1978.

[5] D. J. Roulston and M. H. Elsaid, "Comer Currents in p+-n-n+ Diodes with n+ Isolation Diffusions," *IEEE Trans. Electron Devices,* vol. 25, no. 11, pp. 1327-1328, 1978.

[6] E. L. Heasell, "Diffusion in Ideal Cylindrical and Spherical Junctions-Apparent Diffusion Lenth," *IEEE Tran. Electron Devices,* vol. 27, no. 9, pp. 1771-1777, 1980.

[7] P.-J. Chen, K. Misiakos, A. Neugroschel and F. A. Lindholm, "Analytical Solution for Two-Dimensional Current Injection from Shallow p-n Junctions," *IEEE Trans. Elecron Devices,* vol. 32, no. 11, pp. 2292-2296, 1985.

[8] F. V. D. Wiele and E. Demoulin, "Inversion layers in Abrupt p-n junctions," *Solid-State Electron,* vol. 13, no. 6, pp. 717-726, 1970.

[9] M. S. Tyagi, Introduction to Semiconductor Materials and Devices, New York,NY,USA: Wiley, 2004.

[10] TCAD Sentaurus User Manual, Synopsys, 2013.

[11] A. S. V. Sarma and S. Ahmad, "RF current distribution across metal-semiconductor ohmic contacts in mm-wave IMPATTs," *Solid-State Electronics,* vol. 38, no. 6, pp. 1209-1214, 1995.

[12] R. W. Dutton and R. J. Whittier, "Forward Current-Voltage and Switching Characteristics of p+-n-n+ (Epitaxial) Diodes," *IEEE Trans. Electron Devices,* vol.

16, no. 5, pp. 458-467, 1969.

[13] R. C. Thomas, An Analytical Model of the DC and Frequency Dependent 2-D and 3-D Current Spreading in Forward biased Shallow P-N Junctions, M.S Thesis, Indian Institue of Technology,Madras, 2014.

[14] P. V. Mohan, Spreading resistance models for electrical /thermal applications, M.S. Thesis,Indian Institue of Technology,Madras, 2006.

APPENDIX

A1. Sentaurus Device editor Command file

```
;Reinitializing SDE
(sde:clear)

;Defining Variables
(define Lp @Lp@)
(define Ln @Ln@)
(define an @an@)
(define Deltan @deltan@)
(define Jd @Jd@)
(define Wn @Wn@)
(define pdope @p_doping@)
(define ndope @n_doping@)
(define p_contact @<an*Lp-Jd>@)

(sdegeo:set-default-boolean "BAB")

;Defining p-region
(sdegeo:create-cuboid
(position 0 0 0)  (position (* an Lp) Jd (* an Lp)) "Silicon" "p-region")

;Defining p-contact dummy box
(sdegeo:create-cuboid
(position 0.0 0.0 0.0) (position p_contact -0.1 p_contact) "Aluminum" "dummy")

;Defining Contact sets
(sdegeo:define-contact-set "p-side" 4.0  (color:rgb 1.0 0.0 0.0 ) "##" )
(sdegeo:define-contact-set "n-side" 4.0  (color:rgb 1.0 1.0 0.0 ) "||" )

;Definining n-region
(sdegeo:create-cuboid
(position 0 0 0)  (position (+  (* an Lp) (* Deltan Lp)) (* Wn Lp) (+  (* an Lp) (* Deltan
Lp))) "Silicon" "n-region")

;Setting Contacts
(sdegeo:set-current-contact-set "n-side")
(sdegeo:define-3-D-contact (find-face-id
(position (/ (+  (* an Lp) (* Deltan Lp)) 2.0) (* Wn Lp) (/ (+  (* an Lp) (* Deltan Lp))
2.0))) "n-side")
(sdegeo:set-current-contact-set "p-side")
(sdegeo:set-contact (find-body-id
(position (/ p_contact 2.0) -0.05 (/ p_contact 2.0))) "p-side")
(sdegeo:delete-region (find-body-id (position (/ (* an Lp) 2) -0.05 (/ (* an Lp) 2))))

(render:rebuild)
(sdeio:save-tdr-bnd (get-body-list) "@tdrboundary/o@")
```

A2. Sentaurus Mesh File

```
Definitions {
        Constant "Constant.nreg" {
        Species = "PhosphorusActiveConcentration"
        Value = @n_doping@
        }
        Constant "Constant.preg" {
        Species = "BoronActiveConcentration"
        Value = @p_doping@
        }
}
Placements {
        Constant "PlaceCD.nreg" {
        Reference = "Constant.nreg"
        EvaluateWindow {
        Element = region ["n-region"]
                }
        }
        Constant "PlaceCD.preg" {
        Reference = "Constant.preg"
        EvaluateWindow {
        Element = region ["p-region"]
                }
        }
}
```

```
Definitions {

        Refinement "global.all" {

        MaxElementSize = ( !(puts [expr (@an@+@deltan@)*@Lp@/10.0])! !(puts
[expr (@Wn@)*@Lp@/10.0])! !(puts [expr (@an@+@deltan@)*@Lp@/10.0])!)

        MinElementSize = ( !(puts [expr (@an@+@deltan@)*@Lp@/10.0])! !(puts
[expr (@Wn@)*@Lp@/10.0])! !(puts [expr (@an@+@deltan@)*@Lp@/10.0])!)

        RefineFunction = MaxLengthInterface(Interface("n-region","p-region"),
        Value = 0.001, Factor = 1.5, UseRegionNames)

        RefineFunction = MaxLengthInterface(Interface("n-region","nside"),
        Value = 0.001, Factor = 1.5, UseRegionNames)

        }

        Refinement "Ref.pregion" {

        MaxElementSize = (!(puts [expr (@an@)*@Lp@/10.0])! !(puts [expr
@Jd@/10.0])! !(puts [expr (@an@)*@Lp@/10.0])!)

        MinElementSize = (!(puts [expr (@an@)*@Lp@/10.0])! !(puts [expr
@Jd@/10.0])! !(puts [expr (@an@)*@Lp@/10.0])!)

        }

        Multibox "MB.pregiony" {

        MaxElementSize = ( !(puts [expr (@an@)*@Lp@/10.0])! !(puts [expr
@Jd@/10.0])! !(puts [expr (@an@)*@Lp@/10.0])!)

        MinElementSize = ( !(puts [expr (@an@)*@Lp@/10.0])! 1e-4 !(puts [expr
(@an@)*@Lp@/10.0])! )

        Ratio = ( 1.0 -1.35 1.0)

        }

        Multibox "MB.pregionx" {

        MaxElementSize = ( !(puts [expr (@an@)*@Lp@/10.0])! !(puts [expr
@Jd@/10.0])! !(puts [expr (@an@)*@Lp@/10.0])!)

        MinElementSize = ( 1e-4 !(puts [expr @Jd@/10.0])! !(puts [expr
(@an@)*@Lp@/10.0])! )

        Ratio = ( -1.35 1.0 1.0)
        }
```

```
        Multibox "MB.pregionz" {

        MaxElementSize = ( !(puts [expr (@an@)*@Lp@/10.0])! !(puts [expr
@Jd@/10.0])! !(puts [expr (@an@)*@Lp@/10.0])!)

        MinElementSize = ( !(puts [expr (@an@)*@Lp@/10.0])! !(puts [expr
@Jd@/10.0])! 1e-4 )

        Ratio = ( 1.0 1.0 -1.35)

        }
}

Placements {

        Refinement "Place.all" {

        Reference = "global.all"

        RefineWindow = Material ["Silicon"]

        }

        Refinement "Place.pregion" {

        Reference = "Ref.pregion"

        RefineWindow = Region ["p-region"]

        }

        Multibox "PlaceMB.pregiony" {
        Reference = "MB.pregiony"
        RefineWindow = Cuboid [(0 !(puts [expr @Jd@-0.002])! 0) (!(puts [expr
@an@*@Lp@])! @Jd@ !(puts [expr @an@*@Lp@])!)]
        }

        Multibox "PlaceMB.pregionx" {
        Reference = "MB.pregionx"
        RefineWindow = Cuboid [(!(puts [expr @an@*@Lp@-0.002])! 0 0) (!(puts [expr
@an@*@Lp@])! @Jd@ !(puts [expr @an@*@Lp@])!)]
        }

        Multibox "PlaceMB.pregionz" {
        Reference = "MB.pregionz"
        RefineWindow = Cuboid [(0 0 !(puts [expr @an@*@Lp@-0.002])!) (!(puts [expr
@an@*@Lp@])! @Jd@ !(puts [expr @an@*@Lp@])!)]
        }
}
```

A3. Sentaurus Device Command file

a) DC simulation

```
File{
        Grid = "@tdr@"
        Parameter = "@parameter@"
        Current = "n@node@"
        Plot    = "n@node@"
        Output  = "n@node@"
}

Electrode{
        {Name="p-side"      Voltage=0.55} *Bias voltage
        {Name="n-side"      Voltage=0.0 hRecVelocity = @hRec@} *boundary condition
}

Physics{
  Mobility(
  DopingDependence
  )
  Recombination(
  SRH(DopingDependence)
  )
}

Plot {
  eDensity hDensity eCurrent hCurrent Current
  Potential SpaceCharge ElectricField
  eMobility hMobility eVelocity hVelocity
  Doping DonorConcentration AcceptorConcentration
  ConductionBandEnergy ValenceBandEnergy hquasifermienergy equasifermienergy
}

Math {

  Extrapolate
  Iterations=10
  NotDamped=10
  DirectCurrent
  RelErrControl
  ErRef(Electron)=1.e10
  ErRef(Hole)=1.e10
  Digits=10             * relative error control value. Iterations stop if dx/x < 10^(-Digits)
  Method=ILS            * use the iterative linear solver with default parameter
  Transient=BE          * switches on BE transient method
  Number_Of_Threads=maximum
  Number_Of_Solver_Threads=maximum
  Number_Of_Assembly_Threads=maximum
```

```
}

Solve {
  *- Build-up of initial solution:
  NewCurrentPrefix="init"
  Coupled(Iterations=100){ Poisson }
  Coupled(Iterations=100){ Poisson Hole }
  Coupled(Iterations=100){ Poisson Electron Hole }


  *-  gate voltage sweep
  NewCurrentPrefix="IV_"
  Quasistationary(
        InitialStep=1e-6 Increment=1.5
    MinStep=1e-5 MaxStep=1e-3
    Goal{ Name="p-side" Voltage= 0.55 } *bias voltage
   ){ Coupled{ Poisson Electron Hole }
   CurrentPlot(Time=(Range=(0 1) Intervals=100))
  }
}
```

b) Small-signal Simulation

```
Device DIODE{
        File{
        Grid = "@tdr@"
        Parameter = "@parameter@"
        Current = "n@node@"
        Plot    = "n@node@"
        }
        *initial voltage and boundary condition
        Electrode{
        {Name="pside"         Voltage=0.55}
        {Name="nside"         Voltage=0.0 hRecVelocity = @hRec@}
        }

        Physics{
          Mobility(
          DopingDependence
          )
          Recombination(
          SRH(DopingDependence)
          )
        }

        Plot {
          eDensity hDensity eCurrent hCurrent Current
          Potential SpaceCharge ElectricField
          eMobility hMobility eVelocity hVelocity
          Doping DonorConcentration AcceptorConcentration
          ConductionBandEnergy ValenceBandEnergy hquasifermienergy
```

```
equasifermienergy
        }
}
Math {

 Extrapolate
 Iterations=10
 NotDamped=10
 DirectCurrent
 RelErrControl
 ErRef(Electron)=1.e10
 ErRef(Hole)=1.e10
 Digits=10            * relative error control value. Iterations stop if dx/x < 10^(-Digits)
 Method=ILS           * use the iterative linear solver with default parameter
 Transient=BE         * switches on BE transient method
 Number_Of_Threads=maximum
 Number_Of_Solver_Threads=maximum
 Number_Of_Assembly_Threads=maximum
}
File {
  Output  = "@log@"
  ACExtract = "@acplot@"
}

System {
 DIODE diode1 (pside=g nside=s)
 Vsource_pset vp ( g 0 ){ dc = 0.55 }
 Vsource_pset vn ( s 0 ){ dc = 0 }
}

Solve {
  *- Build-up of initial solution:
  NewCurrentPrefix="init"
  Coupled(Iterations=100){ Poisson }
  Coupled(Iterations=100){ Poisson Hole }
  Coupled(Iterations=100){ Poisson Electron Hole }

  *-  gate voltage sweep
  NewCurrentPrefix="IV_"
  Quasistationary(
        InitialStep=0.005 Increment=1.3
     MinStep=1e-04 MaxStep=0.05
     Goal{ parameter=vp.dc Voltage= 0.55 }
    ){ ACCoupled (
     StartFrequency=1e2 EndFrequency=1e11 NumberOfPoints=35 Decade
     Node(g s) Exclude(vp vn)
     ACCompute (Time = (Range = (0 1)  Intervals = 1))
   ){ Poisson Electron Hole }
 }
}
```

A4. Matlab code to evaluate F3D for given geometry and boundary conditions.

```
function op = F3d(ax,ay,deltax,deltay,Wn,cf,f,S)
    tau_p = 0.5e-6;     % Minority carrier lifetime
    Dp = 11.27;         % Diffusion Coefficient
    Lp = 24e-4;         % Diffusion length
    alpha = S*Lp/Dp;    % Normalized hole recombination velocity
    omega = 2*pi*f;     % Angular Frequency
    L = sqrt(1+1i*omega*tau_p); % L= √(1 + jωτ_p)
```

Double summation term in (4.8)

```
    F3d4 = 0;    % To perform infinite summation, iterations are done
till increment ≤ 1e-9
    % Every iteration of loop takes two terms to account for the fact
that alternate terms are negative
    inc1 = ones(30,1);                      % Increment value for
summation on n1
    n1 = 1;                                 % Initialization
    while max(abs(inc1))>= 1e-9             % Loop on n1
        l11 = n1*pi/(ax+deltax);            % Lambda1 for n1
        l12 = (n1+1)*pi/(ax+deltax);        % Lambda1 for n1+1
        F3d4_old1 = F3d4;                   % Preserve previous term to
calculate error on n1

        % Summation on n2 for n1
        inc2 = ones(30,1);                  % Increment for summation
on n2
        n2 = 1;                             % Initialization
        while abs(max(inc2)) >= 1e-9        % Loop on n2
            l21 = n2*pi./(ay+deltay);       % Lambda2 for n2
            l22 = (n2+1)*pi./(ay+deltay);   % Lambda2 for n2+1
            k121 = sqrt((l11/L).^2+(l21/L).^2+1);   % K12 for n2
            k122 = sqrt((l11/L).^2+(l22/L).^2+1);   % K12 for n2+1
            F3d4_old2 = F3d4;               % Preserve previous term to
calculate error on n2
            % This statement adds next two terms to the previous term
            F3d4 = F3d4 +
sin(l11*ax).*sin(l21*ay).*cos(l11*ax*cf).*cos(l21*ay*cf).*((alpha/k121+
coth(k121*Wn*L))/(1+alpha*coth(k121*Wn*L)/k121))./(n1*n2*pi^2*sqrt((l11
/L)^2+(l21/L).^2+1))...
+sin(l11*ax).*sin(l22*ay).*cos(l11*ax*cf).*cos(l22*ay*cf).*((alpha/k122
+coth(k122*Wn*L))/(1+alpha*coth(k122*Wn*L)/k122))./((n2+1)*n1*pi^2*sqrt
```

```
((l11/L)^2+(l22/L).^2+1));
            inc2 = abs(F3d4 - F3d4_old2); % Error term for summation on
n2
            n2 = n2+2;                    % Increase n2 by 2
        end

        % Summation on n2 for n1+1
        n2 = 1;                           % Initialization
        inc2 = ones(1,30);
        while max(abs(inc2)) >= 1e-9      % Loop on n2
            l21 = n2*pi./(ay+deltay);     % Lambda2 for n2
            l22 = (n2+1)*pi./(ay+deltay); % Lambda2 for n2+1
            k121 = sqrt((l12/L).^2+(l21/L).^2+1);   % K12 for n2
            k122 = sqrt((l12/L).^2+(l22/L).^2+1);   % K12 for n2+1
            F3d4_old2 = F3d4;             % Preserve previous term to
calculate error on n2
            % This statement adds next two terms to the previous term
            F3d4 =
F3d4+sin(l12*ax).*sin(l21*ay).*cos(l12*ax*cf).*cos(l21*ay*cf).*((alpha/
k121+coth(k121*Wn*L))/(1+alpha*coth(k121*Wn*L)/k121))./(n2*(n1+1)*pi^2*
sqrt((l12/L)^2+(l21/L).^2+1))...

+sin(l12*ax).*sin(l22*ay).*cos(l12*ax*cf).*cos(l22*ay*cf).*((alpha/k122
+coth(k122*Wn*L))/(1+alpha*coth(k122*Wn*L)/k122))./((n2+1)*(n1+1)*pi^2*
sqrt((l12/L)^2+(l22/L).^2+1));
                inc2 = abs(F3d4 - F3d4_old2);
            n2 = n2+2;                    % Increase n2 by 2
        end
        inc1 = abs(F3d4 - F3d4_old1);     % Increment for summation
on n1
        n1 = n1+2;                        % Increment n1 by 2
    end
```

Summation on n_2 in (4.8)

```
    F3d3 = 0;                             % Summation term
    inc1 = 1;                             % Increment
    n2 = 1;                               % Initialization
    while abs(max(inc1)) >= 1e-9          % Loop on n2
        l1 = n2*pi./(ay+deltay);          % Lambda2 for n2
        l2 = (n2+1)*pi./(ay+deltay);      % Lambda2 for n2+1
        k11 = sqrt(1+(l1/L).^2);          % k2 for n2
        k12 = sqrt(1+(l2/L).^2);          % k2 for n2+1
```

```
        m = ax/(ax+deltax);                 % Constant term
        F3d3_old = F3d3;                    % Preserve previous term to
calculate error
        % This statement adds two new terms to previous term
        F3d3 = F3d3
+m*((sin(l1*ay).*cos(l1*cf*ay)).*((alpha/k11+coth(k11*Wn*L))/(1+alpha*c
oth(k11*Wn*L)/k11))./(n2*pi*sqrt(1+(l1/L).^2))...
               +
m*((sin(l2*ay).*cos(l2*cf*ay)).*((alpha/k12+coth(k12*Wn*L))/(1+alpha*co
th(k12*Wn*L)/k12)))./((n2+1)*pi*sqrt(1+(l2/L).^2));
        inc1 = abs(F3d3 - F3d3_old);        % Error term
        n2 = n2+2;                          % Increase n2 by 2
    end
```

Summation on n_1 in (4.8)

```
    F3d2 = 0;                               % Summation term
    inc1 = 1;                               % Increment
    n1 = 1;                                 % Initialization
    while abs(max(inc1)) >= 1e-9            % Loop on n1
        l1 = n1*pi/(ax+deltax);             % Lambda2 for n1
        l2 = (n1+1)*pi/(ax+deltax);         % Lambda2 for n1+1
        k11 = sqrt(1+(l1/L).^2);            % k1 for n1
        k12 = sqrt(1+(l2/L).^2);            % k1 for n1+1
        m = ay./(ay+deltay);                % Constant term
        F3d2_old = F3d2;                    % Preserve previous term to
calculate error
        % This statement adds two new terms to previous term
        F3d2 = F3d2
+m.*((sin(l1*ax)*cos(l1*cf*ax))*((alpha/k11+coth(k11*Wn*L))/(1+alpha*co
th(k11*Wn*L)/k11)))/(n1*pi*sqrt(1+(l1/L)^2))...
               +
m.*((sin(l2*ax)*cos(l2*cf*ax))*((alpha/k12+coth(k12*Wn*L))/(1+alpha*cot
h(k12*Wn*L)/k12)))/((n1+1)*pi*sqrt(1+(l2/L)^2));
        inc1 = abs(F3d2 - F3d2_old);        % Increment
        n1 = n1+2;                          % Increase n1 by 2
    end

    F3d1 = ax*ay./((ax+deltax)*(ay+deltay));    %Constant term
    op =
(F3d1+(2*F3d2+2*F3d3+2*2*F3d4)*((1+alpha*coth(Wn*L))/(alpha+coth(Wn*L))
)).^-1; % Final value of F3D

end
```

PULICATIONS BASED ON THIS REPORT

Shubham Jain, Vijaya Kumar Gurugubelli, and Shreepad Karmalkar, "An Analytical Model of the Frequency Dependent 3-D Current Spreading in Forward Biased Shallow Rectangular P-N Junctions", under review in *IEEE Trans. Electron Devices*.